


Article

A Practice-Oriented Proposal to Consider the Flange Effect in Equivalent Frame Modeling of Masonry Buildings

Serena Cattari *, Sara Alfano and Sergio Lagomarsino 

Department of Civil, Chemical and Environmental Engineering, University of Genoa, 16145 Genoa, Italy

* Correspondence: serena.cattari@unige.it

Abstract: This paper focuses on the so-called “flange effect” in unreinforced masonry buildings when the connection among walls is good, thus forming a 3D assembly of intersecting piers (with L-, C-, T-, or I-shaped cross-sections). Given the direction of the horizontal seismic action, the presence of such flanges (the piers loaded out-of-plane) can influence the response of the in-plane loaded pier (the web) in terms of failure modes, maximum strength, and displacement capacity. Specific rules are proposed in codes to evaluate the effective width of the flange, for the in-plane verification of a single masonry wall. However, in the case of 3D equivalent frame (EF) modeling of the whole building, all the intersecting piers should be considered entirely, to model the response in both the orthogonal directions as well as the torsional behavior, but this may lead to overestimating the flange effect if a perfect connection is assumed. This paper investigates the capability of simulating the actual behavior in EF models by introducing an elastic shear connection at the intersection between two piers using an “equivalent beam”, coupling the nodes at the top of piers. A practice-oriented analytical formulation is proposed to calibrate such a flange effect on the basis of the geometric features and material properties of the web and the flange. Its reliability is tested at the scale of simple 3D assemblies and entire buildings as well. Finite element parametric analyses on masonry panels with symmetrical I- and T-shaped cross-sections have been performed to investigate the axial load redistribution between the flanges and the web and the consequent repercussion on the overall performance of the web. The results have proven that, after a calibration of the shear connection, the variation of axial force between the web and the flanges is correctly reproduced and the strength criteria for 2D panels provide reliable results. Finally, in the conclusions, some practical hints for simulating an imperfect wall-to-wall connection are also provided, since this case is relevant in historic masonry buildings, which are characterized by different masonry types, transformations over time, and already-cracked conditions.

Keywords: flange effect; masonry buildings; equivalent frame model; seismic response



Citation: Cattari, S.; Alfano, S.; Lagomarsino, S. A Practice-Oriented Proposal to Consider the Flange Effect in Equivalent Frame Modeling of Masonry Buildings. *Buildings* **2023**, *13*, 462. <https://doi.org/10.3390/buildings13020462>

Academic Editors: Bora Pulatsu, Semih Gonen and Fulvio Parisi

Received: 9 December 2022

Revised: 1 January 2023

Accepted: 2 February 2023

Published: 8 February 2023



Copyright: © 2023 by the authors. Licensee MDPI, Basel, Switzerland. This article is an open access article distributed under the terms and conditions of the Creative Commons Attribution (CC BY) license (<https://creativecommons.org/licenses/by/4.0/>).

1. Introduction

The modeling of existing unreinforced masonry (URM) buildings addressed to seismic assessment is affected by many uncertainties. Those ascribable to aleatory variables (e.g., mechanical parameters, as discussed in [1]) are the ones most commonly included, but epistemic uncertainties play a crucial role as well (see [2–5]). Examples of epistemic uncertainties for URM buildings are the stiffness of diaphragms and their connection to masonry walls, the effectiveness of the wall-to-wall connection, the actual efficiency of structural aseismic devices such as tie-rods, etc. Although the accurate knowledge of the building under examination constitutes the first essential requisite to properly address the modeling choices [6,7], the capability of models to simulate the large variety of structural details and configurations that may be observed in any single existing building is likewise crucial to correctly transfer these data into numerical simulations.

Recently, [8] provided a comprehensive review of the critical aspects of the nonlinear modeling of URM structures, covering various modeling strategies (i.e., equivalent frame

(EF) approaches and 2D and 3D finite element (FE) procedures based on continuous, discrete, and micro-mechanical approaches, as also classified in [9]) and various aspects (i.e., in-plane and out-of-plane responses of masonry, the wall-to-wall connection, the diaphragm's role).

Among the latter ones, and particularly in the case of EF models, which this paper focuses on, the modeling capability of properly accounting for the effectiveness of the wall-to-wall connection emerged as one of the most relevant requisites. In fact, if the connection between walls is good, a possible redistribution of forces among intersecting piers may occur, generating the so-called “flange effect” (i.e., forming piers with L-, C-, T-, or I-shaped cross-sections). This effect potentially affects both the in-plane and the out-of-plane strength of URM walls, since both depend on the axial load, but this paper focuses only on the repercussions on their in-plane response.

Various experimental campaigns conducted both at the scale of single masonry panels [10–15] and at the structural level [16–19] highlighted potential issues associated with the “flange effect”. In addition, various numerical investigations based on refined FE models highlighted the relevance of the topic [20,21]. However, these works have investigated the issue more at the scale of single components than from the perspective of systematically assessing the repercussions at a global scale or for deriving simplified modeling strategies to be implemented in EF models, as instead is the main goal of this paper.

One relevant outcome is that, especially in the presence of big flanges, it is not correct to consider all the width as effective. Many contributions are present in the literature [22–24] that are addressed in determining the effective flange width in shear walls made by reinforced concrete and reinforced masonry, while very few are the ones focused on URM buildings. In [25], a simplified expression has been proposed that aims to assess the compressive length in the presence of flanged sections. In [26], a simple geometric approach based on the “rule of the 45°” has been outlined for the identification of the effective flange width in URM walls. Instead, in [27], empirical rules have been proposed that establish the effective width as “N” times the thickness of the web (s in Figure 1a), where the value of N is differentiated as a function of the effectiveness of the wall-to-wall connection (if poor, average, or good) and the position of the piers connected (if at a corner—leading to an L-section shape—or at an internal intersection—leading to a T-section shape) (see Figure 1a). Furthermore, indications are provided by the codes [28,29], which substantially depend on the geometry of the interacting walls. Figure 1b illustrates those proposed in Eurocode 6 [28] and adopted as a reference in this paper for the applications illustrated in Sections 4 and 5. In particular, according to such criteria, the length of any interacting wall that may be considered to act as a flange is the thickness of the shear wall plus, on each side of it, where appropriate, the lesser of the following:

- (i) $h_{tot}/5$, where h_{tot} is the overall height of the shear wall;
- (ii) Half the distance between the shear walls (when connected by the intersecting wall), l_s ;
- (iii) The distance to the end of the wall;
- (iv) Half the clear height (h);
- (v) Six times the thickness of the intersecting wall, t .

The numerical simulations available in the literature [4,5,30] confirmed that the adoption of different approaches for modeling orthogonal walls in the EF models (i.e., perfect coupling or total decoupling between them) may produce significant differences in results, such as causing even different outcomes of the design/assessment; these differences are mainly related to those consequent into the pushover curves generated by nonlinear static analyses to interpret the global response of a 3D building. According to what has been recently reviewed by [8] (where further details are provided), Figure 2 illustrates the alternative modeling options commonly adopted in EF models to simulate the connection among intersecting piers:

- Case (a)—the perfect kinematic coupling, by connecting the two piers to the same node, thanks to a rigid offset (the result is a condensation of the total number of degrees of freedom);

- Case (b)—the use of a rigid link;
- Cases (c) and (d)—the adoption of “equivalent elastic beams”, which allow different degrees of connection to be simulated;
- Cases (e) and (f)—the stiffness of the in-plane loaded pier is perfectly connected to an orthogonal pier with an effective width, which is assumed to be the collaborating part of the flange [27]; depending on the direction of loading, the “effective flange width” considered collaborating with the “web” of the composite section may vary (as shown in Figure 2, cases (e) for a shear force in the y-direction and (f) for the x-direction);
- Case (g)—the connection between the orthogonal walls is modeled through zero-length elements; this is the approach adopted in the equivalent frame model proposed by [31,32] and implemented in OpenSees [33].

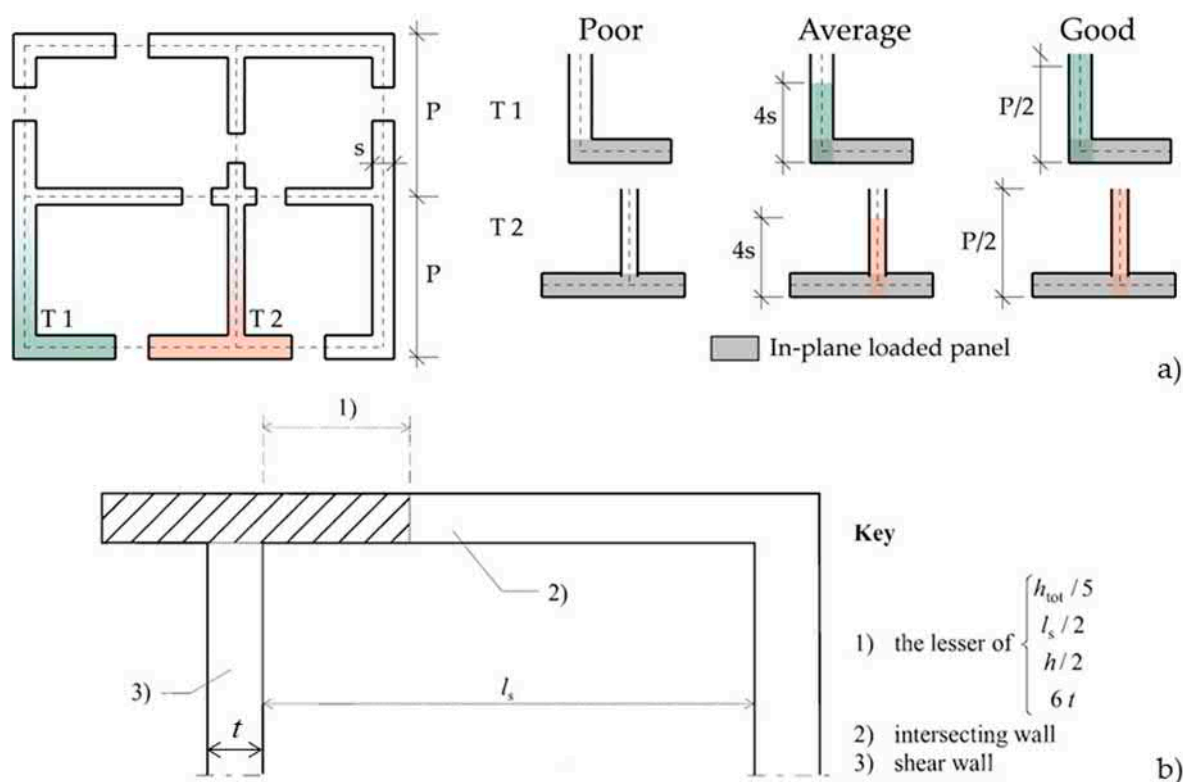


Figure 1. Criteria for defining the effective width for the flange as proposed in the following: (a) [27], the corner case—L-section shape—is marked in green while the internal intersection—T-section shape—is marked in pink; and (b) Eurocode 6, Part 1-1 [28] (adapted from the corresponding references).

Among these alternative strategies, options (c) and (d) illustrated in Figure 2 appear to be an effective and practice-oriented approach to managing this epistemic uncertainty, because all piers are included in the EF model with the total size and the partial contribution to the flange effect is not modeled by considering an effective width but by assuming an elastic shear connection between the intersecting piers, through an equivalent beam. However, there are no specific indications in the literature about how to properly calibrate the stiffness of these beams, accounting for the geometry and materials of collaborating masonry portions, nor whether this approach allows for proper reproductions of both the stiffness and strength of the 3D configuration. In [5,30], some practical applications of calibration are reported with the aim of defining the following: firstly, an “upper bound value” of the stiffness of the equivalent beams able to reproduce the same solution obtained in the case of perfect coupling; secondly, a “lower bound value” corresponding to the case of fully decoupled walls. Once these limits values are defined, a sensitivity analysis may be performed to quantify the influence of various levels of effectiveness of the wall-

to-wall connection on pushover curves' results. In [5], it has been also proven that, if consistent hypotheses are adopted, different software packages and alternative options lead to analogous results.

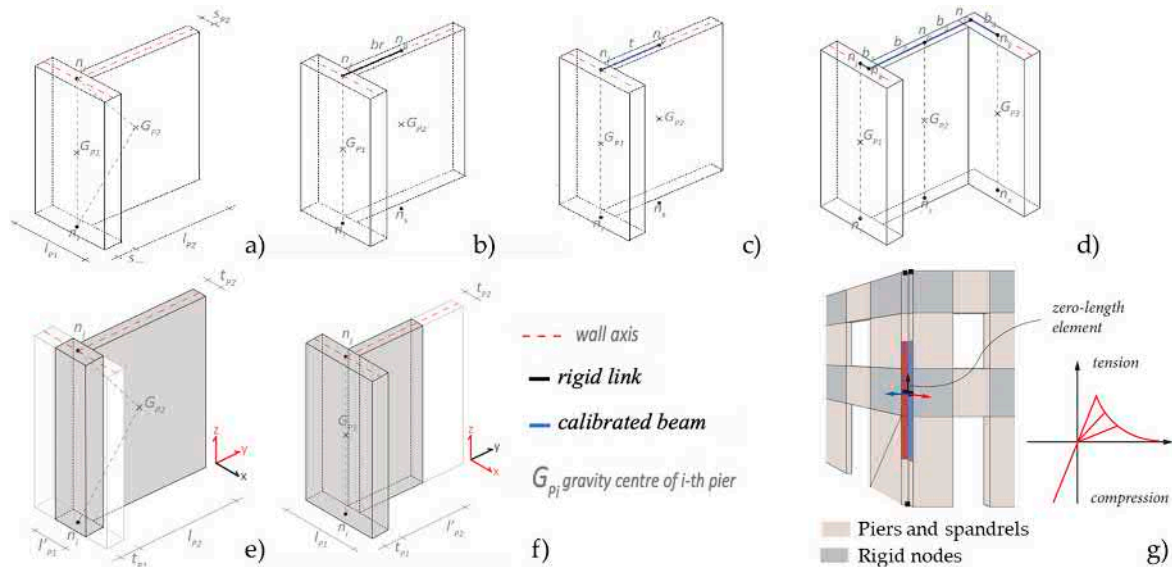


Figure 2. Alternative modeling options for simulating the wall-to-wall connection if equivalent frame models are used (adapted from [8]): (a) perfect kinematic coupling with a rigid offset; (b) rigid link; (c,d) equivalent elastic beams; (e,f) modeling of effective width the collaborating part of the flange; (g) zero-length elements.

Such an approach presupposes that the strength verification of piers may still refer to the rectangular section responding in-plane (a) by considering the influence of the flange only for the computation of the normal stress redistribution. Moreover, a systematic consideration of the effective width of flanges depending on their dimensions is not included (b) and, in most cases, the full coupling is assumed by default options of the software package by considering that all of the flange may interact, regardless of its actual dimension; this may produce an overestimation of the flange effect, since it is unrealistic to consider all the width as effective, especially if it is significant. Indeed, hypotheses (a) and (b) are still debated in the literature. For example, in [26] an analytical model to evaluate the in-plane response of URM piers with single-flange and fixed-free conditions has been formulated. According to this proposal, a specific model—based on a proper modification of that called the “effective pier model”—is developed to investigate the effects of flanges on the lateral strength of a non-rectangular section URM pier. Through this “modified” effective pier model, the maximum strength is computed in the case of the cantilever pier on the basis of four primary failure modes, namely rocking, bed-joint sliding, toe crushing, and diagonal tension. This model was successively revised by [13] considering the case of piers with flanges on both ends.

Within this general context, the goal of this paper is twofold. Firstly, the research question on the suitability of using the in-plane strength criteria proposed in the literature for piers with a rectangular section even in the presence of flanges is discussed (Section 3). To this aim, the results of nonlinear finite element analyses of simple systems are used as a reference (Section 2). Secondly, a practice-oriented analytical formulation is proposed to assess the stiffness of the equivalent beam to be introduced for reproducing the flange effect (Section 4). Finally, the effectiveness of such a formulation is tested by using both simple systems (Section 5), characterized by piers with T- or I-shaped cross-sections and complex 3D structures inspired by real URM existing buildings (Section 6). In all these cases, nonlinear analyses are made by adopting equivalent frame models developed by the Tremuri software package version 2.2.20 [34].

2. Examined Configurations and Reference Solutions by Finite Element Modeling

The examined case studies (Figure 3) are represented by three I- and T-shaped sections, hereinafter referred to as I-1, I-2, I-3, T-1, T-2, and T-3.

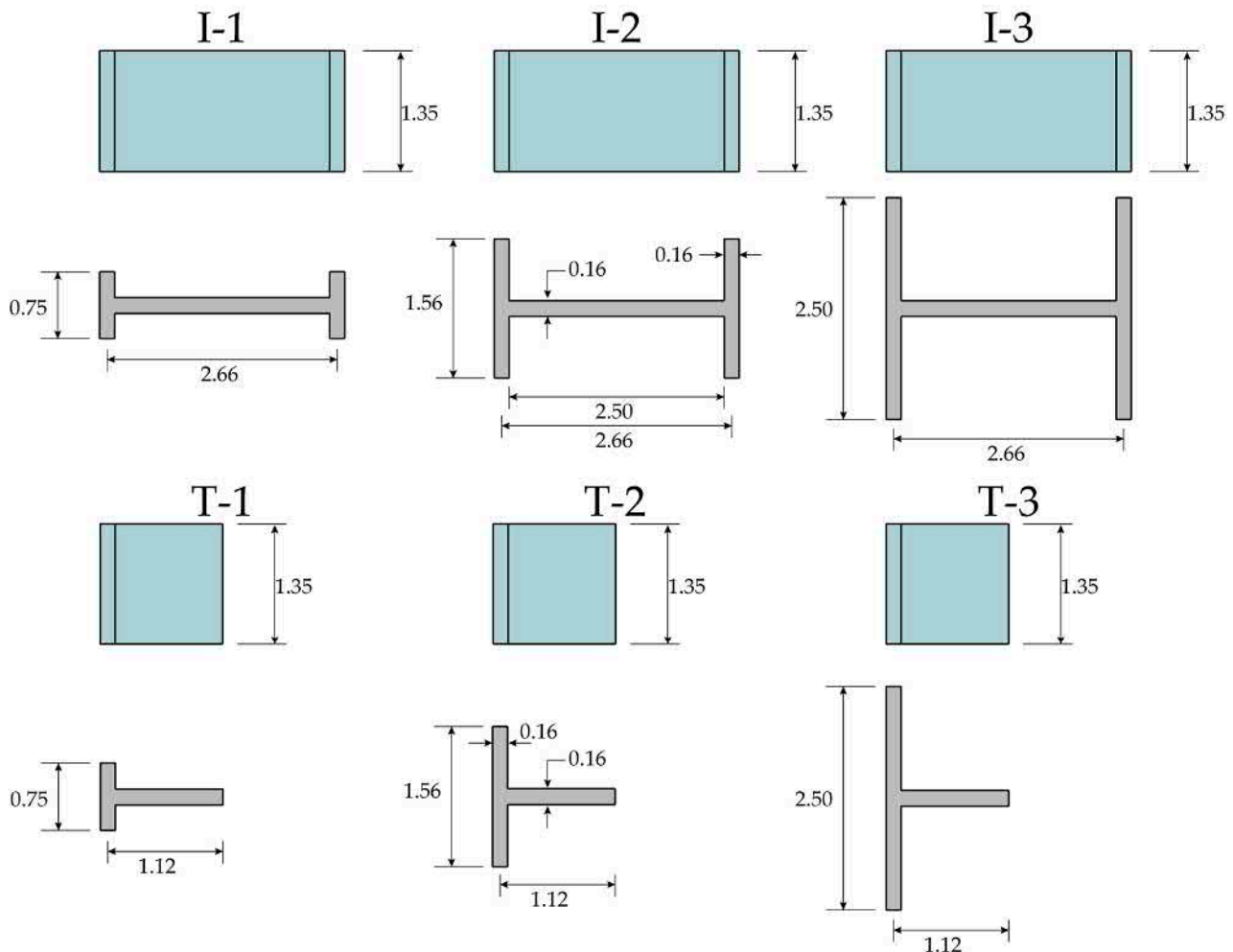


Figure 3. Case study structures: I- and T-shaped flanged sections with varying lengths of the flange (in meters).

The web panel always has the same geometry while the dimension of the flanges is progressively increased passing from I-1 to I-3. As a consequence, the resulting sections are characterized by different relative ratios of axial stiffness and flexural stiffness between the flanges and the web.

All the introduced case studies were modeled using both of the following:

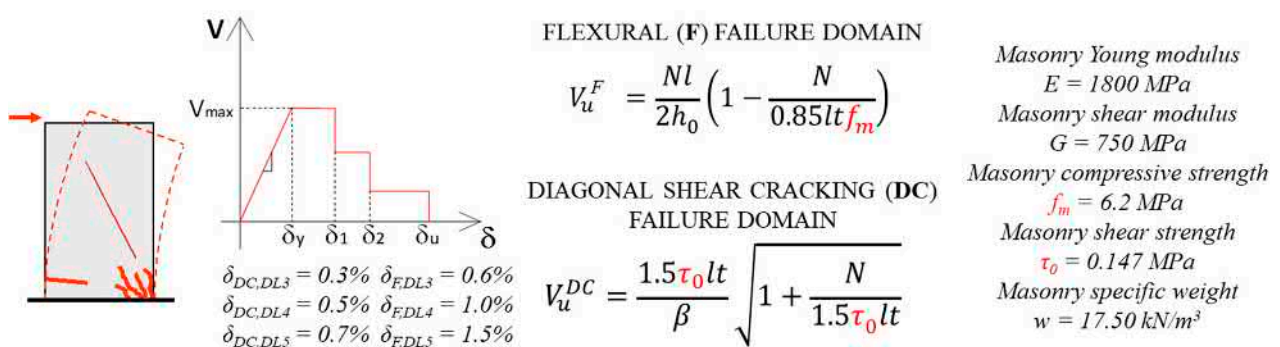
- In ABAQUS, by using the Concrete Damage Plasticity (CDP) model [35] and fully integrated ($2 \times 2 \times 2$ integration points) 8-node linear brick elements;
- In Tremuri [34], by using the multilinear constitutive law for masonry panels proposed by [36] and recently validated by simulating the actual response of complex buildings in [37–39].

The CDP model is an isotropic model that uses concepts of damaged elasticity in combination with tensile and compressive plasticity. The uniaxial stress–strain curves in tension and compression represent the main input of the constitutive law (which depends on the variables summarized in Table 1) and two distinct damage variables in tension (d_t) and compression (d_c) are introduced. Although the model was originally developed for concrete and isotropic quasi-brittle materials, since then it has been successfully used also in many applications addressing the analysis of masonry structures [40–43].

Table 1. Values of the analyzed compression levels.

	$(\sigma/f_c)_1$	$(\sigma/f_c)_2$	$(\sigma/f_c)_3$	$(\sigma/f_c)_4$ [%]	$(\sigma/f_c)_5$	$(\sigma/f_c)_6$	$(\sigma/f_c)_7$
Cantilever	-	1.8	3.4	5.0	8.3	14.7	24.4
Fixed–fixed	0.9	1.8	3.4	5.0	8.3	14.7	24.4
	σ_1	σ_2	σ_3	σ_4 [N/mm ²]	σ_5	σ_6	σ_7
	0.05	0.1	0.2	0.3	0.5	0.9	1.5

As highlighted in [44] and [8], a crucial point in using finite element models—especially if used as a reference for a consistent comparison with other modeling strategies such as the EF models—is the proper calibration of the parameters on which the adopted constitutive law is based. In this paper, the calibration of parameters is based on the procedure outlined by specific steps in [8] and in-depth exemplified in [45]. The calibration is made at the scale of single panels characterized by a rectangular cross-section (panel 1, $1.12 \times 0.16 \times 1.35 \text{ m}^3$ and panel 2, $2.66 \times 0.16 \times 1.35 \text{ m}^3$) and by assuming as “target behavior” for the calibration the one predicted by simplified code-based strength criteria available in the literature [46,47] to interpret the main failure modes that are expected to occur in masonry piers. The latter are the ones usually implemented in the EF model that directly work at the panel scale. In particular, the following strength criteria have been assumed as a reference in this research: the one proposed by [48] for interpreting the diagonal shear cracking failure mode; the one adopted in the Italian Structural Code [49] for interpreting the flexural failure mode. These criteria are illustrated in Figure 4 together with their analytical expressions. Then, the calibration procedure presupposes a comparison of the response of the pier simulated by the FE model not only in terms of strength but also in terms of the elastic stiffness, post-peak behavior, and displacement capacity estimated for different values of the applied axial load. Interested readers are invited to refer to [45] for further details, while Figure 5 summarizes the values herein adopted as resulting from such a calibration process. Moreover, in this phase, a set of preliminary analyses aimed at assessing the influence of the mesh dimension on the convergence process has also been performed. It led to the adoption of a geometry of the brick elements approximatively equal to $10 \times 10 \times 12.5 \text{ cm}$, which provides almost the same results in terms of base shear-displacement curves and occurred damage of a more refined mesh, guaranteeing at the same time a higher computational efficiency.

**Figure 4.** Strength criteria were adopted as “target strength behavior” for the calibration process (adapted from [8]).

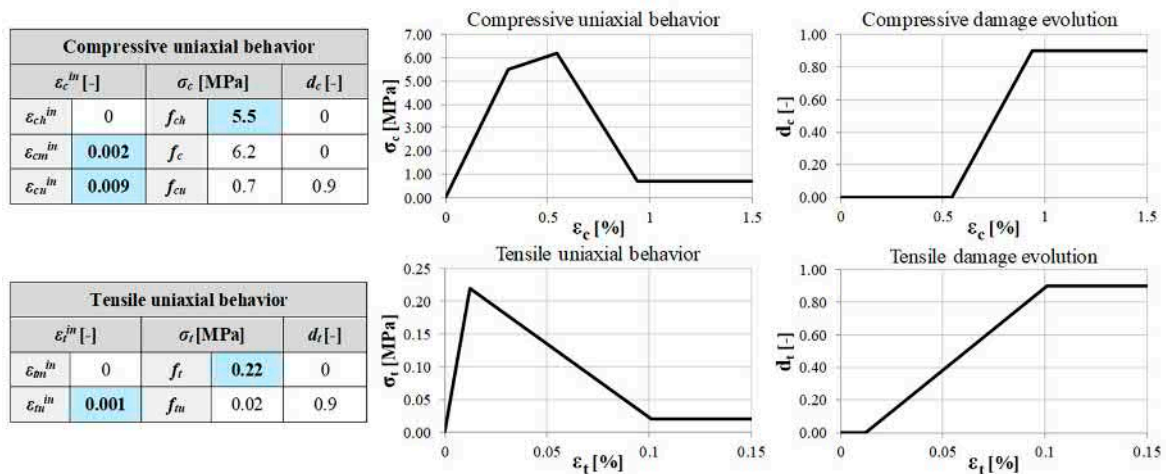


Figure 5. Uniaxial behavior for the compressive and tensile regimes determined through the calibration for the CDP model and summary of adopted parameters (where f_t —tensile strength of the material and f_{ch} —uniaxial compressive stress corresponding to the point of initial yield; ε_{cm} —value of uniaxial compressive strain corresponding to the reaching of the maximum strength; ε_{cu} —value of the uniaxial compressive strain corresponding to the end of the softening branch).

Moreover, Figure 6 shows the outcome of such a calibration for the two panels, by referring to both configurations of cantilever and fixed–fixed end rotation and varying the axial load applied on the top of piers. The results show a very good agreement between the numerical simulations carried out through the FE and EF models, demonstrating the capability of the CDP model to correctly reproduce the failure domain of URM piers without flanges.

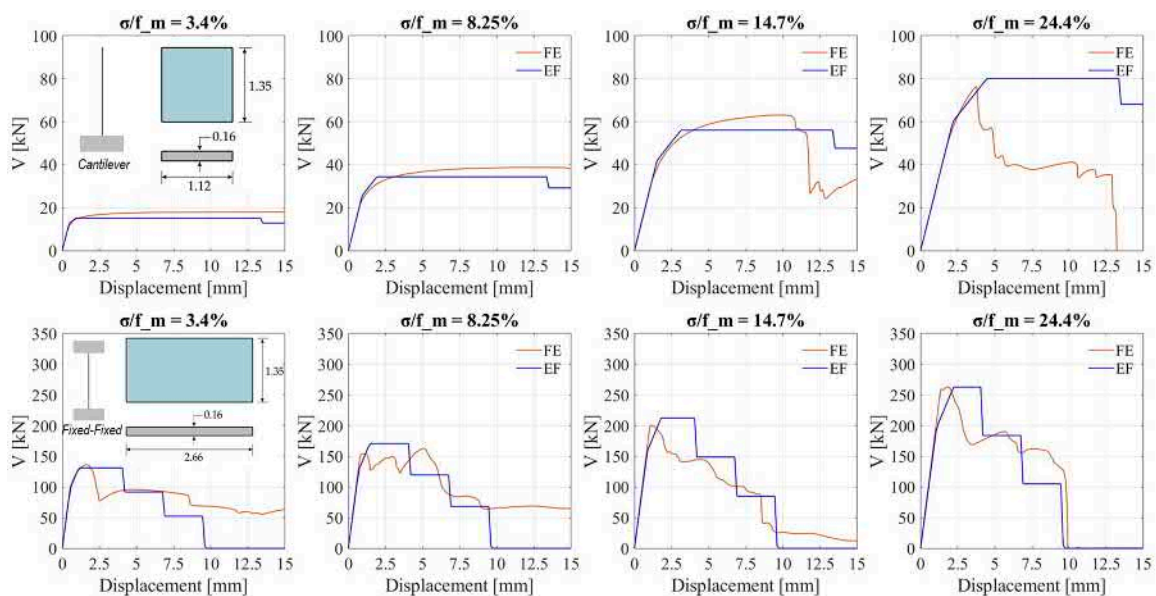


Figure 6. Comparison of the base shear-displacement curves of masonry piers adopted for the calibration process varying the acting compressive stress state.

Once the calibration process was completed, the same parameters were adopted for the numerical simulation of the simple schemes in Figure 3. Moreover, for them, both the cantilever and the fixed–fixed end rotation configurations have been analyzed. Lateral load monotonic analyses were performed under the assumption of control displacement and by considering different increasing compression levels σ/f_c . The applied values are

reported in Table 1, in particular, in the case of the cantilever boundary condition, six values $((\sigma/f_c)_i, i = 1, \dots, 6)$ were explored; for the fixed–fixed scheme, a further value has been considered to better investigate the region of the failure domain associated with flexural failure. The vertical load was always applied only on the web; consequently, the flanges bear just their weight.

3. Preliminary Analyses Made by the FE Models to Address the Legitimacy of Using the in-Plane Strength Criteria for Piers with a Rectangular Cross-Section

This section debates the legitimacy of using the in-plane strength criteria proposed in the literature for piers with a rectangular section.

To this aim, after the execution of the lateral load FE analyses on all configurations introduced in Section 2, (see also [50] for some preliminary results on I-shaped systems), the following entities were determined:

- The maximum total base shear ($V_{y,tot}$), as the sum of the reaction forces at the base of the whole section (i.e., including flanges);
- The maximum base shear ($V_{y,W}$), as the sum of the reaction forces associated only with the web panel.

Figure 7 illustrates the comparison between the failure domain of the web panel and the values of $V_{y,tot}$ (black dots) and $V_{y,W}$ (white dots), respectively, as estimated by the performed FE analyses. The failure domain is defined through the strength criteria illustrated in Figure 4.

The values of $V_{y,tot}$ and $V_{y,W}$ represented in Figure 7 correspond to the axial load value N_{app} evaluated as the sum of the axial load applied at the top section and half the web weight. This is equivalent to assume that the vertical load applied at the top section remains on the web panel without any redistribution between the web and the flanges.

From these graphs, the following emerges:

- The distance in the vertical direction between each black dot and the corresponding white dot quantifies the contribution to the global strength given by the flanges. This contribution is not always modeled in models based on the EF approach; therefore, in this way, the associated error may be quantified. It comes out that, by accounting also the contribution of the flanges, the maximum base shear increases, on average, by 15%; such a result is, in percentage, substantially similar for both the static schemes and the different applied axial loads that have been investigated. However, it should be highlighted that in the case of flanges with higher width (which is plausible, for example, in the presence of old masonry buildings) this contribution may be more significant. As also discussed in [5], the contribution of panels loaded “out-of-plane” may be neglected for walls with thicknesses lower than 0.4 m, by providing anyhow conservative results. Conversely, for greater thicknesses, such contribution progressively becomes more significant; thus, neglecting it could lead to appreciable variations in the pushover curve, in terms of the overall base shear capacity, initial stiffness, and also ultimate displacement capacity.
- White dots correspond to the values of $V_{y,W}$, which are those that have to be compared with the failure domain of the web panel represented in the graphs. In particular, it is possible to observe that, in the initial part of the domain, they are higher than the predictions of the flexural failure criterion. That especially happens for the I-2 and I-3 configurations (where the flange is longer); conversely, it is less significant when the flange is rather short (I-1). This phenomenon occurs in both the considered static schemes, even if it is more pronounced in the presence of the cantilever boundary condition, since in this case the part of the domain with a prevailing flexural response is more extended.
- By examining the part of the domain mainly affected by the shear failure, the $V_{y,W}$ values are almost in agreement with the predictions of the shear failure criterion in the case of the fixed–fixed static scheme, while they are always lower when considering the cantilever boundary condition.

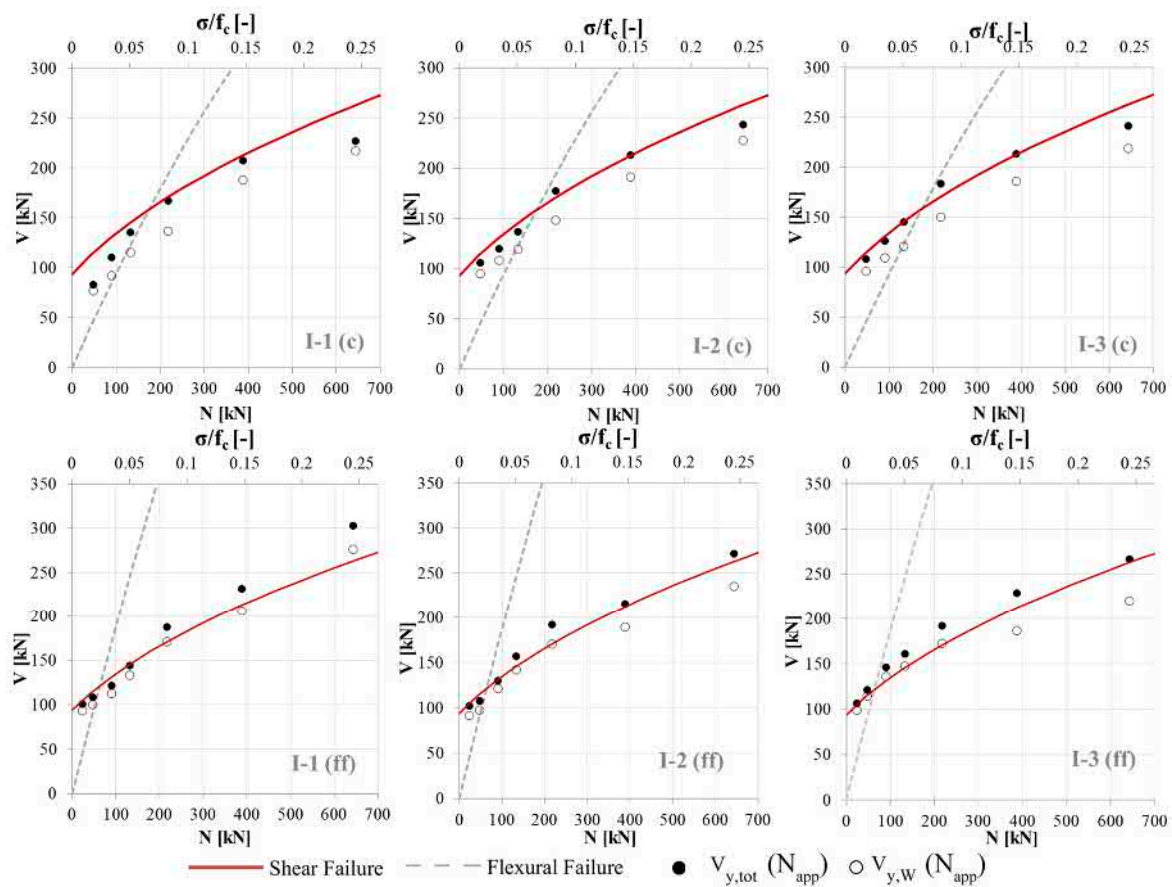


Figure 7. Failure domain of the web panel and results of the numerical FE analyses. Results refer to each one of the examined configurations (“c” = cantilever scheme; “ff” = fixed-fixed scheme); the values of $V_{y,tot}$ and $V_{y,W}$ correspond to the axial force N_{app} .

In Figure 8, a different type of representation is proposed by way of example for the case of the cantilever static scheme. More specifically, the values of $V_{y,W}$ (white dots) are represented in correspondence with the actual axial load acting after the application of the vertical loads in the mid-section of the web panel ($N_{W,eff}$). $N_{W,eff}$ was computed from the FE model by integrating the vertical stresses on the mid-cross-section of the web. Conversely, the values of $V_{y,tot}$ (black dots) are still represented as in the previous graph and, therefore, in correspondence of N_{app} . This explains the shifting between the black and the white dots, which refer to the same analysis.

In this way, by examining the white dots, it is possible to see the actual axial load and the actual maximum base shear referring to the web panel. That is of main interest in the view of an EF approach where pier panels are modeled as in-plane elements and the behavior of a flanged section addresses the correct estimate of the shear and the normal force acting on the in-plane loaded panel.

The results in Figure 8 highlight the following:

- The distance in the horizontal direction between the white and the black dot, for a fixed analysis, provides a measure of the difference between the actual axial load acting in the mid-section of the web ($N_{W,eff}$) and the axial load that would act in this section if no redistribution between the web and the flanges occurred ($N_{W,app}$). Since this difference is not negligible, this result suggests that the axial load applied at the top section of the web redistributes, moving in part to the two flanges. This effect is visible for all the configurations, and thus for all the examined length of the flange; however, it is slightly higher when considering I-2 and I-3 than in the case in which the flange is shorter (I-1);

- By looking at the dots representing $V_{y,W}$, which are now referred to the correct value of axial load acting on the web panel, it may be observed that they correctly reproduce, in all the three examined configurations, the strength domain of the web panel. This is particularly true when the highest values of applied vertical load are examined (i.e., where, according to the strength domain, the shear failure is expected);
- The discrepancies in the initial part of the domain already observed in the previous graphs are still present and even emphasized. For low applied axial loads, the values of $V_{y,W}$ are higher than what was expected; that is particularly evident for the configurations where the flange is longer (I-2 and I-3). In both these cases, they are closest to the shear failure criterion instead of the flexural one.

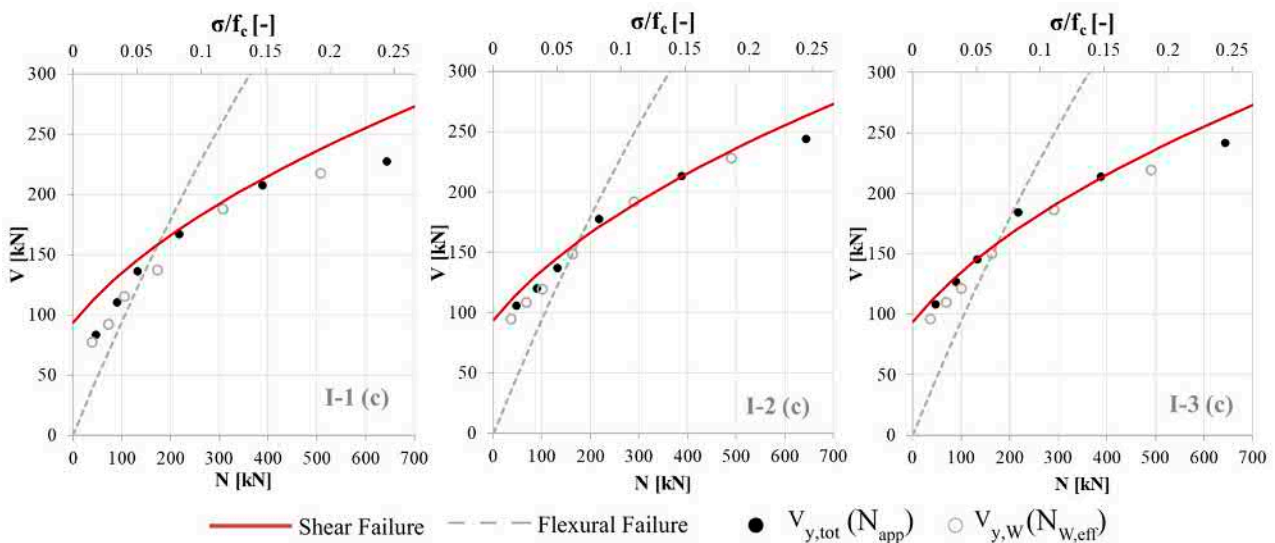


Figure 8. Failure domain of the web panel compared with the results of the numerical FE analyses for each one of the introduced case study structures (cantilever scheme); the values of $V_{y,tot}$ are represented in correspondence of N_{app} , while the values of $V_{y,W}$ are represented in correspondence of $N_{W,eff}$.

This last observation can be explained by considering that the presence of the flange tends to inhibit the flexural failure of the web panel, avoiding the associated rocking mechanism. Consequently, when applying low axial loads, the web is interested in the development of shear cracks rather than pure flexural failures, which is interested only by the base section partialization. This especially happens when the length of the flange is higher (I-2, I-3); in fact, in these cases, thanks to its not negligible weight compared to that of the web, the flange provides a more significant contribution to counterbalance the overturning of the web panel. Conversely, when the length of the flange is significantly lower than that of the web (I-1), the inhibition of the flexural failure does not happen. That is confirmed by Figure 8, where the values of $V_{y,W}$ (white dots) in the initial part of the domain are substantially closer to the flexural failure criterion; the slight overestimation is justified by the fact that the constitutive model employed in the FE analyses also includes the tensile strength of the material, while the strength criterion adopted for the flexural failure neglects this contribution.

These observations are confirmed by the damage pattern detected in I-1, I-2, and I-3 (cantilever static scheme), which is illustrated in Figure 9 for two different values of applied axial load ($(\sigma/f_c)_2$ and $(\sigma/f_c)_4$). The results obtained for I-1 when applying $(\sigma/f_c)_2$ point out a pure flexural failure occurs, with the partialization of almost all the base section.

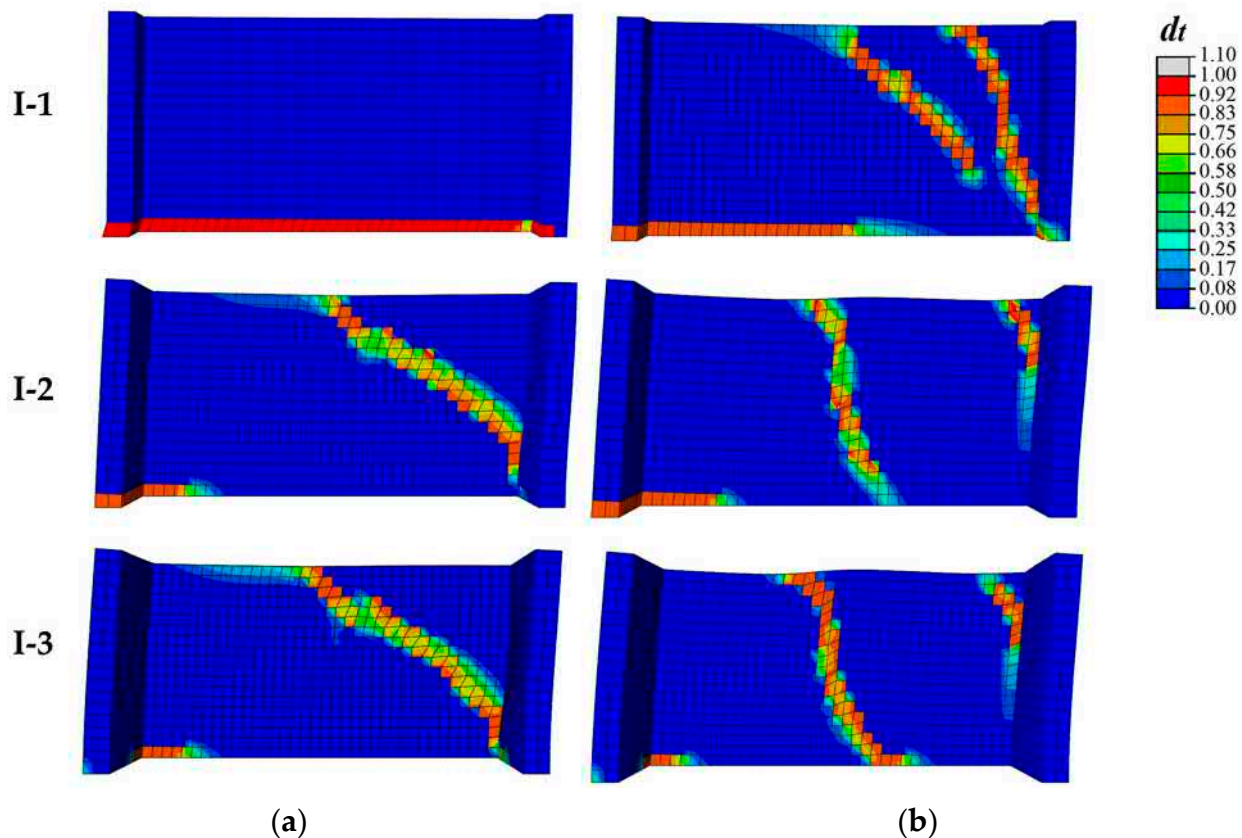


Figure 9. Tensile damage contour plots obtained from the FE analyses performed on the introduced I-shaped panels (cantilever scheme): (a) applied axial load $(\sigma/f_c)_2$; (b) applied axial load $(\sigma/f_c)_4$.

This is consistent with the fact that, as already observed, the associated value of $V_{y,W}$ is substantially close to the predictions of the flexural strength criterion (Figure 8). Moving to I-2 and I-3, it is worth noting that, even for the lowest applied vertical load $((\sigma/f_c)_2)$, which corresponds to the very beginning of the failure domain, the web panels are already interested in the development of shear cracks, and a pure flexural failure does not occur; this is due to the flange subjected to tension that minimizes the rocking phenomenon and the partialization of the base section of the web. For a higher level of applied axial load $((\sigma/f_c)_4)$, in I-1 shear cracks start to develop, but the partialization of the base section is still evident and still interests quite a significant part of the base section; conversely, in I-2 and I-3 an almost vertical crack develops starting from the center of the panel.

The results examined in this section stress that, by assuming to the ability to effectively capture the actual axial load acting in the web panel, the strength criteria currently adopted in the EF models for the in-plane loaded panel can almost correctly predict its maximum strength. Therefore, the main issue to be addressed is the actual EF model's capability of evaluating the actual vertical load acting on the web panel after the redistribution that occurs between it and the flanges. That is important and of primary relevance after the application of the dead loads and, possibly, also during the analysis. The second part of this paper is addressed to deepen this issue.

Finally, the results suggest that, when the flange is sufficiently long compared to the in-plane loaded panel, the flexural criterion is likely to not develop and only the one describing the shear failure should be used, also for the lower values of the applied vertical load. A more in-depth investigation of this aspect is out of the scope of this paper, but these results outline useful directions for orienting experimental tests in the future. As a confirmation of that, other works from the literature confirm this result [14].

4. Proposal of the Practice-Oriented Analytical Formulation

This section proposes a practice-oriented analytical formulation to calibrate the equivalent stiffness of the shear connection between two orthogonal piers, simulated by beams in an equivalent frame model. This shear connection depends on the relative size and position of the two piers, and it is not rigid even in the case of a complete masonry interlocking, since the complex 3D assembly of the piers should not behave as a single beam with the conservation of a plane section. This shear connection may be obtained by the equivalent beams introduced in Figure 2 (cases (c) and (d)).

In the case of the minimum assembly constituted by two orthogonal piers (characterized by width— l — and thickness— t), depending on the horizontal load direction, one will act as a web (the one mainly behaving in-plane) and the other as a flange. Figure 10 depicts some possible configurations of connected piers, typical of piers at the intersection of external and internal walls (case (a)), at the corner intersection (case (b)) or at the intersection of two internal walls (case (c)). Of course, in the more general case, piers can be connected to another wall at the other end. The problem also depends on the distance d between the centroid of the web (pier that is loaded in-plane) and the middle plane of the flange. In the following, the flange effect refers to the systems of Figure 10 loaded along the X direction. If the direction Y is considered, a flange effect should be considered for cases (b) and (c), by assuming $d = d_y$ and considering the flange and the web are exchanged.

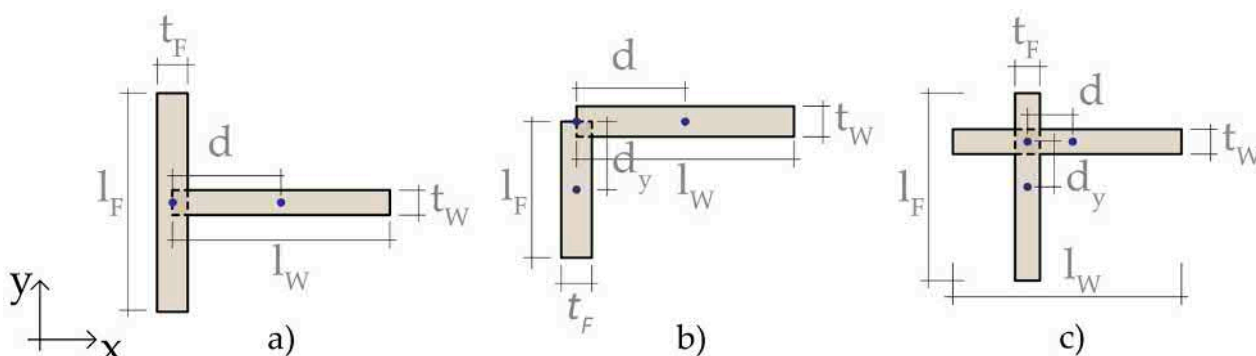


Figure 10. Possible configuration of connected piers: (a) intersection of external and internal walls; (b) corner intersection; (c) intersection of two internal walls.

An analogy may be established between the overall flexural behavior of the 3D assembly of two piers and the case of a composite beam, made by a beam coupled by a slab fixed by shear connectors. In the following, reference has been made to the formulation originally introduced by [51] to analyze the structural behavior of composite wood–concrete beams with flexible shear connectors. The problem was solved by imposing the equilibrium and congruence equations to the composite section of Figure 11a, where the timber beam constitutes the original existing floor and the thin concrete slab is introduced as a strengthening solution. Figure 11b summarizes, from a kinematic and static point of view, the behavior of such a composite section. Under the hypothesis of linear elastic behavior, the differential equations may be expressed as a function of the classic three generalized displacements of the 2D beam, with the addition of the relative displacement δ between the timber and concrete sections. In [51], such an equation has been solved by assuming proper boundary conditions and obtaining a closed-form solution to design the steel shear connectors to be used to guarantee the proper coupling of the two parts.

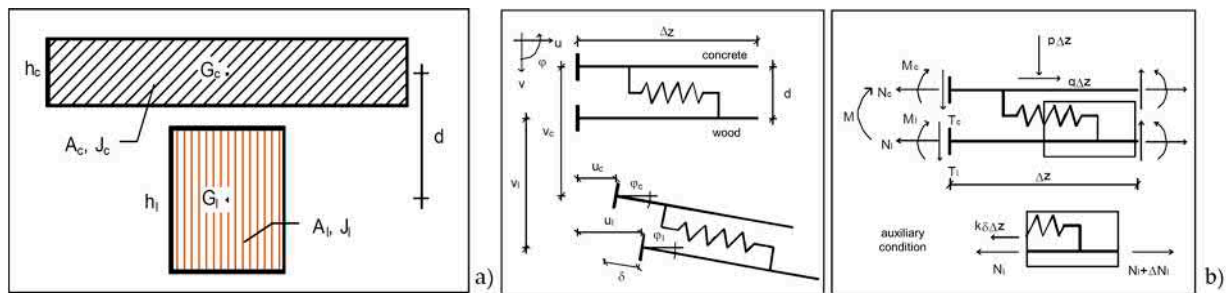


Figure 11. (a) Timber–concrete composite section studied in [51]; (b) kinematic and static variables that regulate the system by referring to an infinitesimal length D_z of the beam.

In the case of a pier with a flange, the question is to evaluate the property of the shear connection (shear stiffness of the beam to be implemented in the equivalent frame model) that can simulate the actual behavior of the 3D assembly of piers. An analogy is established between such a timber–concrete composite section and the web–flange system made by interacting piers; in this case, δ is the relative vertical displacement between the two piers at their intersection, but it represents—as concentrated—the actual deformation of the web and flange piers, which do not maintain a plain section.

Let us introduce K_z , which expresses the stiffness of the “equivalent” shear connection between the two piers, i.e., the stiffness affecting such a vertical relative displacement. By changing such a stiffness, it is possible to pass from the condition of full coupling ($K_z \rightarrow \infty$) to the limit case of almost independent piers ($K_z = 0$). In general, the value of K_z depends on the stiffness of the two piers, the web and the flange, and the distance from the latter to the centroid of the web. Similarly to what was introduced in [51], the dimensionless parameter ω is then introduced to regulate this transition and to account for the geometrical and mechanical variables playing a role in the phenomenon:

$$\omega = \frac{K_z h^2}{E_F A_F} \frac{(1 + \zeta)(E_W J_W + E_F J_F) + d^2 E_F A_F}{E_W J_W + E_F J_F} = \frac{K_z h^2}{E_W A_W} \left(\frac{1 + \zeta}{\zeta} + \frac{12 d^2}{I_W^2 \left(1 + \frac{E_F J_F}{E_W J_W}\right)} \right) \quad (1)$$

where h is the interstory height; A_W and J_W are the area and moment of inertia of the web ($t_W l_W$ and $\frac{1}{12} t_W l_W^3$, respectively); A_F and J_F the area and moment of inertia of the flange ($t_F l_F$ and $\frac{1}{12} l_F t_F^3$, respectively); E_W and E_F are the Young’s moduli of masonry characterizing the two piers; d , as already introduced, is the distance between the centroid of the web and the middle plane of the flange; and finally, $\zeta = \frac{E_F A_F}{E_W A_W}$ is a dimensionless factor. Since the thickness is usually limited—if compared to the width of piers whose flange effect may be relevant ($E_F J_F \ll E_W J_W$)—and by considering that sometimes the out-of-plane stiffness is neglected, the term $E_F J_F / E_W J_W$ may be reasonably assumed to be equal to 0. Under this specific assumption, it results in the following:

$$\omega = \frac{K_z h^2}{E_W A_W} \left(\frac{1 + \zeta}{\zeta} + \frac{12 d^2}{I_W^2} \right) \quad (2)$$

Section 4 illustrates some parametric analyses carried out on simple systems to address reference values to be adopted for ω .

In practical applications made by numerical models, such a shear stiffness is modeled through the equivalent beam connected to the nodes at the top of the web and flange piers; it simulates the interlocking spread along the overall interstory height h . According to the beam theory, the shear stiffness of this beam may be expressed as follows:

$$K_z h = \frac{5 G_W A_B}{6 l_B} \quad (3)$$

where l_B and A_B are the length and the transversal area of the equivalent beam, respectively. The equivalent beam is assumed as made by the same material of the web (shear modulus G_W , Poisson coefficient ν_W). It is then possible to compute the area A_B from Equations (1) or (2):

$$A_B = l_B \omega \frac{12(1 + \nu_W)A_W}{5h \left(\frac{1+\zeta}{\zeta} + \frac{12d^2}{l_W^2 \left(1 + \frac{E_F J_F}{E_W J_W} \right)} \right)} \cong l_B \omega \frac{12(1 + \nu_W)A_W}{5h \left(\frac{1+\zeta}{\zeta} + \frac{12d^2}{l_W^2} \right)} \quad (4)$$

The value of A_B thus depends on the following: the geometrical features of intersecting piers; the distance between the nodes that the beam is connected to (which defines its length l_B); and, through the ω parameter, the degree of connection that has to be introduced in order to consider that the 3D assembly does not behave as a single beam with a flange.

The moment of inertia of the equivalent beam must be very high to make the contribution of the flexural deformability negligible. To this aim, the ratio between flexural and shear stiffness should be assumed to be higher than 10 ($\psi = \frac{12E_W J_B}{l_B^2 G_W A_B} > 10$):

$$J_B > 0.3 l_B^2 A_B \quad (5)$$

As mentioned in the Introduction, the equivalent frame modeling of masonry buildings usually assumes a rigid connection between piers at the intersection of masonry walls, but this overestimates the global stiffness and determines an incorrect estimate of the generalized forces in the two piers, with consequently a wrong evaluation of the failure conditions. Therefore, it is necessary to provide a proper shear connection between the two piers when the flange effect is expected to be relevant, that is, in the following cases:

- (i) If the web (pier loaded in-plane) is characterized by large dimensions;
- (ii) If the distance d is large (in cases (a) and (b) of Figure 10);
- (iii) The flange area is “big” compared to that of the web.

For the evaluation of the proper shear stiffness of the equivalent beam, Equation (4) provides the area, which depends on the geometry and material properties of the 3D assembly, but it is necessary to assume the correct value of the dimensionless parameter ω . In the following section, it is demonstrated, by a comparison between the results for FE and EF models, that a constant reference value of ω may be assumed for all relevant cases.

It is worth noting that in most of the 3D assemblies of masonry piers the calibration of the connecting equivalent beams should be evaluated in both directions, where the web and the flange are exchanged. In the end, only one equivalent beam may be introduced, by adopting as the shear stiffness the lower or the average between the values of K_z in the two directions X and Y , evaluated by Equations (1) or (2).

5. Application of the Formulation to Simple Masonry Piers with Flanges

In the following, the results obtained on the I-shaped 3D assemblies introduced in Section 2 are first examined. It is worth recalling that the FE numerical model simulates a condition of good wall-to-wall connection, and all models refer to the cantilever scheme.

The comparison between the FE and EF models is carried out by adopting different representations to investigate the axial load redistribution effects, namely, the following:

- Figure 12 shows the evolution of the axial load (N) on the three piers of the I-shaped assemblies (I-1, I-2, and I-3), i.e., the web (in blue) and two flanges (in orange, the compressed one, and in red, the one subjected to tension), versus the horizontal displacement applied on the top of the system (d_{top}). The solid line refers to the reference FE solution, while the various dotted lines illustrate the sensitivity of the results to increasing values of ω (i.e., 1, 3, 5, and 100). The results are illustrated for two of the examined compressive stress states (i.e., the ones induced by the axial loads applied on the top of the web corresponding to an average stress σ equal to 0.2 and 0.5 MPa).

- Figure 13 depicts the percentage error of the axial force on the web computed by the EF model just after the application of vertical loads ($d_{top} = 0$) versus the reference value obtained by the FE model. This error is illustrated, for different values of ω , as a function of the investigated average compressive stress.
- Figure 14, analogously to Figure 13, illustrates the percentage error in the estimation of the axial force by also considering its variation until the attainment of the maximum shear on the web panel. The error is estimated by considering the average value within the range of horizontal top displacements from 0 up to 6.75 mm.

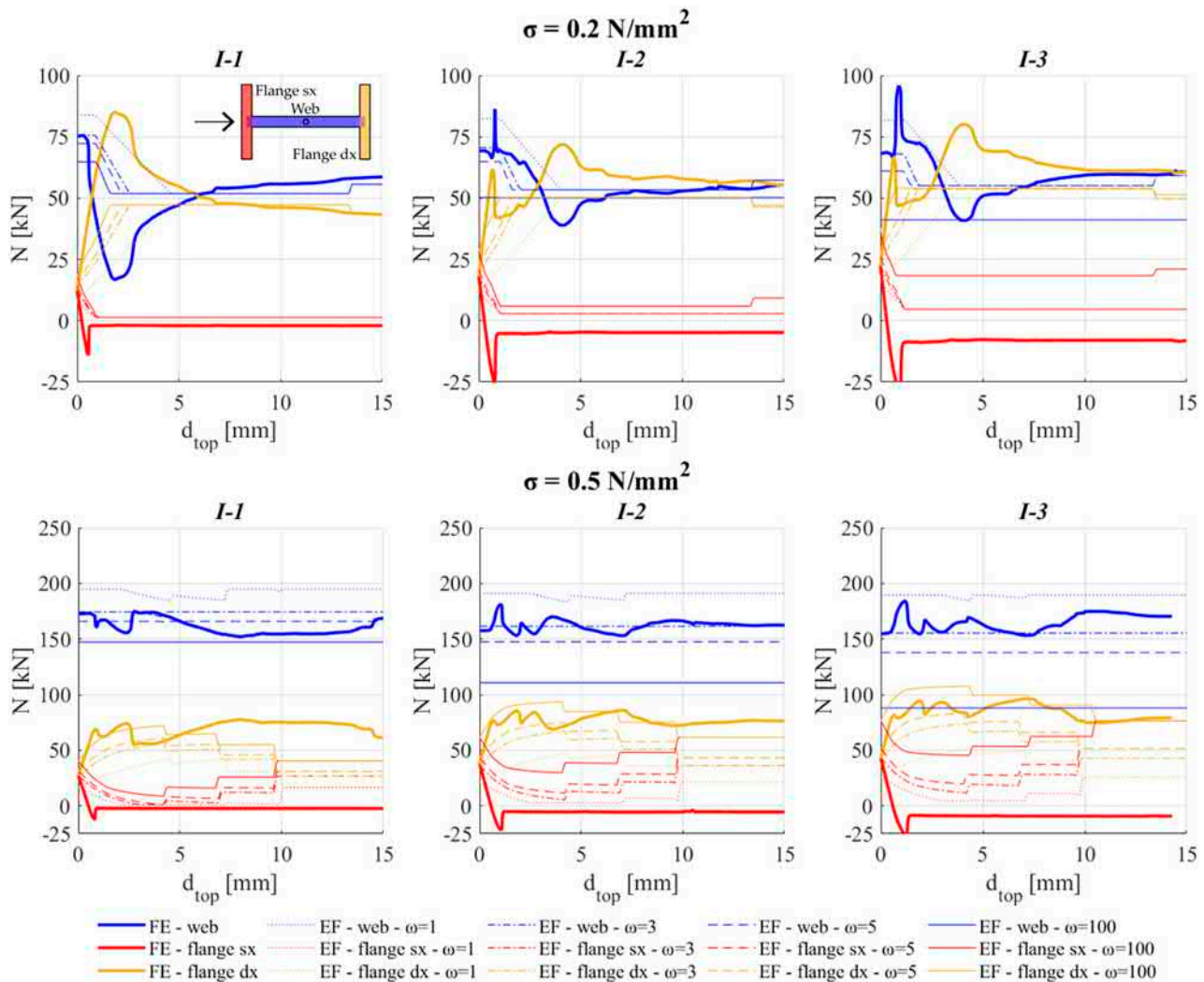


Figure 12. Comparison between FE and EF models in terms of variation of the axial loads on the web and the flanges of I-shaped 3D assembly.

This first set of results addresses the issue concerning the definition of the reference value of ω associated with a good wall-to-wall condition and ability of reproducing the most reliable redistribution of axial forces between the web and the two flanges.

Figure 13 highlights a not negligible effect of ω ; thus, the calibration of the equivalent beam may potentially significantly affect the results. It emerges that the reference value of ω , which minimizes the error, just after the application of the vertical load, is 3. Values higher than 10 and lower than 1 significantly alter the initial redistribution of axial forces alternatively producing a strong underestimation (even higher than 40%) or overestimation (up to 20%) of the axial load acting on the web.

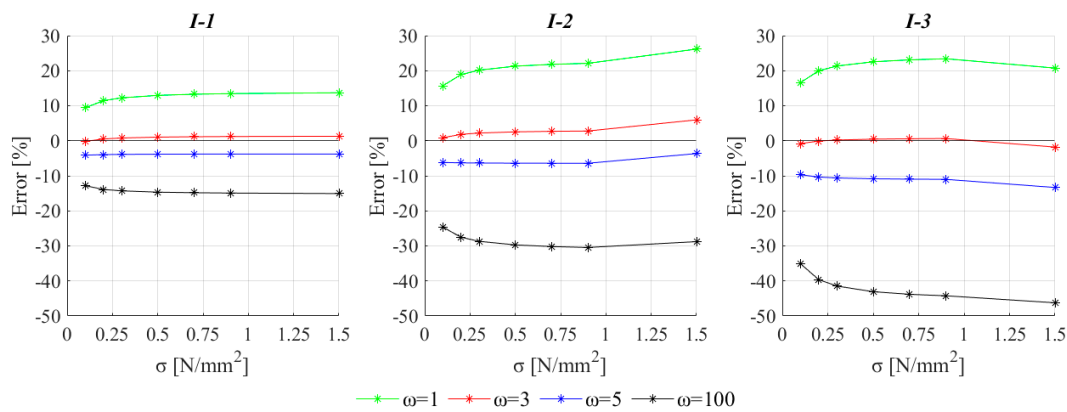


Figure 13. Percentage error on the estimate of the axial load just after the application of vertical loads ($d_{top} = 0$) for the examined I-shaped 3D assembly, as a function of average vertical stress.

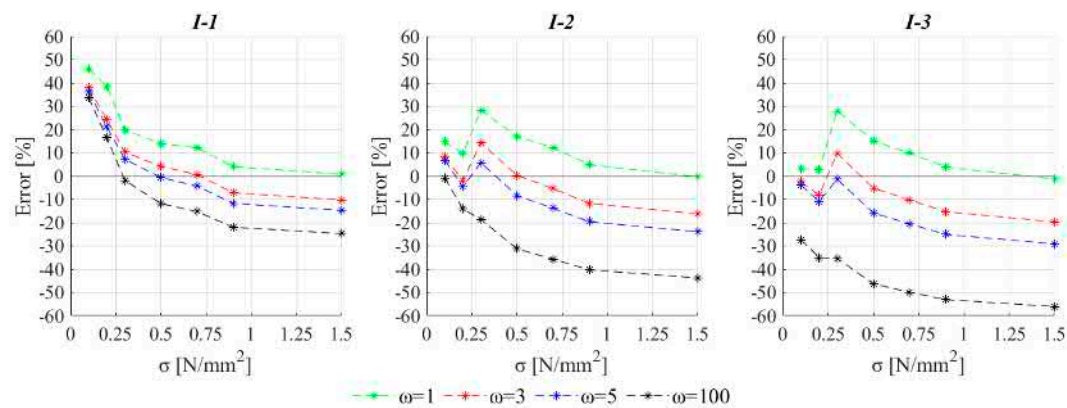


Figure 14. Average percentage error on the estimate of the axial load, considering its variation along the analysis up to $d_{top} = 6.75$ mm, for the examined I-shaped 3D assembly, as a function of average vertical stress.

It has been verified that the value of $\omega = 100$ exactly reproduces the condition of perfect connection, illustrated in Figure 2 by cases (a) and (b). Indeed, in this case, the axial load acting after the application of the dead loads in the web ($N_{W,0}$) and the flanges ($N_{F,0}$) may be easily and analytically estimated as a function of the axial stiffness of each panel:

$$N_{F,0} = N_{TOT} \frac{A_F}{A_W + 2A_F} \quad (6)$$

$$N_{W,0} = N_{TOT} \frac{A_W}{A_W + 2A_F} \quad (7)$$

where N_{TOT} is the total axial load acting at the base section (including the applied vertical load and the total weight of the 3D assembly), A_F is the area of the cross-section of one flange and A_W is the area of the cross-section of the web. Similarly, the bending moment acting on one flange $M_{F,i}$, considering the i -th step of the incremental analysis, may be obtained as follows:

$$M_{F,i} = V_i h \frac{J_F}{J_W + 2J_F} \quad (8)$$

where $V_i h$ is the total bending moment (V_i is the base shear and h the height of the piers), J_W is the moment of inertia of the web panel, with respect to its centroid, and J_F is the moment of inertia of the flange (by considering only the transfer contribution). By considering that $M_{F,i}$ can be expressed also as the product of the axial load variation $\Delta N_{F,i}$ occurring in one flange with respect to $N_{F,0}$ multiplied by its distance with respect to the centroid of the section ($l_W/2$), it is possible to also make explicit the value of $\Delta N_{F,i}$ and thus estimate the

value $N_{F,i}$ of the vertical load acting on the two flanges of the I-shaped cross-section at the i -th incremental step of the application of the horizontal load:

$$N_{F,i} = N_{F,0} \pm \Delta N_{F,i} = N_{F,0} \pm \frac{6l_F V_i h}{I_W^2 + 6l_F l_W} \quad (9)$$

From Figure 12, it emerges that, regarding the transfer of axial forces, the error obtained by considering ω equal to 100 is in particular very relevant from the web to the flange in which the axial force is reduced by the application of the horizontal force. This effect is more evident as the flange increases.

When considering the results referring to the compression level $\sigma = 0.2 \text{ N/mm}^2$ (Figure 12a), the redistribution of N between the web and the flange in compression is, for all the examined case studies, higher than when applying a more significant axial load (Figure 12b). For example, by examining what happens to I-1, it may be noted that, when considering the lower compression level ($\sigma = 0.2 \text{ N/mm}^2$), the significant redistribution between the web and the flange (approximately occurring for d_{top} between 1.5 mm and 2.5 mm) is due to the partialization of the base section of the web panel, which produces a consequent increment of the axial load in the compressed flange. After that, due to a significant concentration of compression damage in the flange (crushing), the axial load comes back to the web ($d_{top} > 2.5 \text{ mm}$). On the contrary, when applying $\sigma = 0.5 \text{ N/mm}^2$, since the rocking mechanism is no more activated, the axial load acting at the base section of the web is almost constant during the analysis and the main redistribution occurs between the two flanges. Such a transfer of actions, which occurs in the case of a low compressive load being applied, is not captured by the EF model; therefore, for low values of σ more significant percentage errors are founded, regardless of the assumed value of ω (see Figure 14).

By summing up, the adoption of a rigid connection produces results in the redistribution effects, which are still acceptable only when the dimension of the flange is limited with respect to the dimension of the web (percentage error with respect to the reference FE solution equal to almost 15%). However, when the dimension of the flange increases with respect to the dimension of the web, this strategy leads to an overestimation of the axial load acting on the flanges and, consequently, to an underestimation of the one acting on the web: the percentage error of the EF approach with respect to the reference solution increases up to 50%. This may imply repercussions appreciable also in the simulation of the seismic response of complex systems as discussed in Section 6.

Figure 15 illustrates the base shear (V_W) versus horizontal top displacement (d_{top}) curve varying the examined I-shaped systems and the assumed values of ω ; the base shear only refers, for both FE and EF models, to the contribution of the web. This figure aims to highlight the repercussions of the estimate of axial load on the strength capacity of the in-plane loaded pier. In the graphs, the dotted orange lines are the equivalent bilinear idealization of the pushover curve obtained by the FE model, just to also refer to a representation more similar to the one provided by the EF model. This idealized curve has been derived by evaluating the following: (i) the initial stiffness at a base shear equal to 0.7 times the maximum value; (ii) the equivalent yield base shear under the hypothesis of imposing the equivalence of the areas under the original curve and the equivalent bilinear, up to a displacement equal to the attainment of the ultimate drift of web ($d_{top} = 6.75 \text{ mm}$). As it is possible to observe, by using the value of ω equal to 3 or 5, the strength capacity is also well captured, as a logical consequence of what is already discussed in Section 3. Figure 16, similarly to Figures 13 and 14, illustrates the percentage error of the estimate of the base shear provided by the EF model computed with respect to the maximum base shear (a) or the equivalent yield base shear (b) of the FE model. Once again, the figure highlights that the adoption of the above-mentioned values for ω allows for also reducing the error in the estimate of the shear strength capacity. Please consider that in the case of low values of the average compressive stress σ , i.e., where the error is still significant regardless of the value adopted for ω , the inconsistency is due to the fact that in the EF

model the strength capacity is estimated as the minimum between the flexural and shear strength criterion while the results discussed in Section 2 suggest that the presence of the flange may alter the occurrence of the pure flexural behavior.

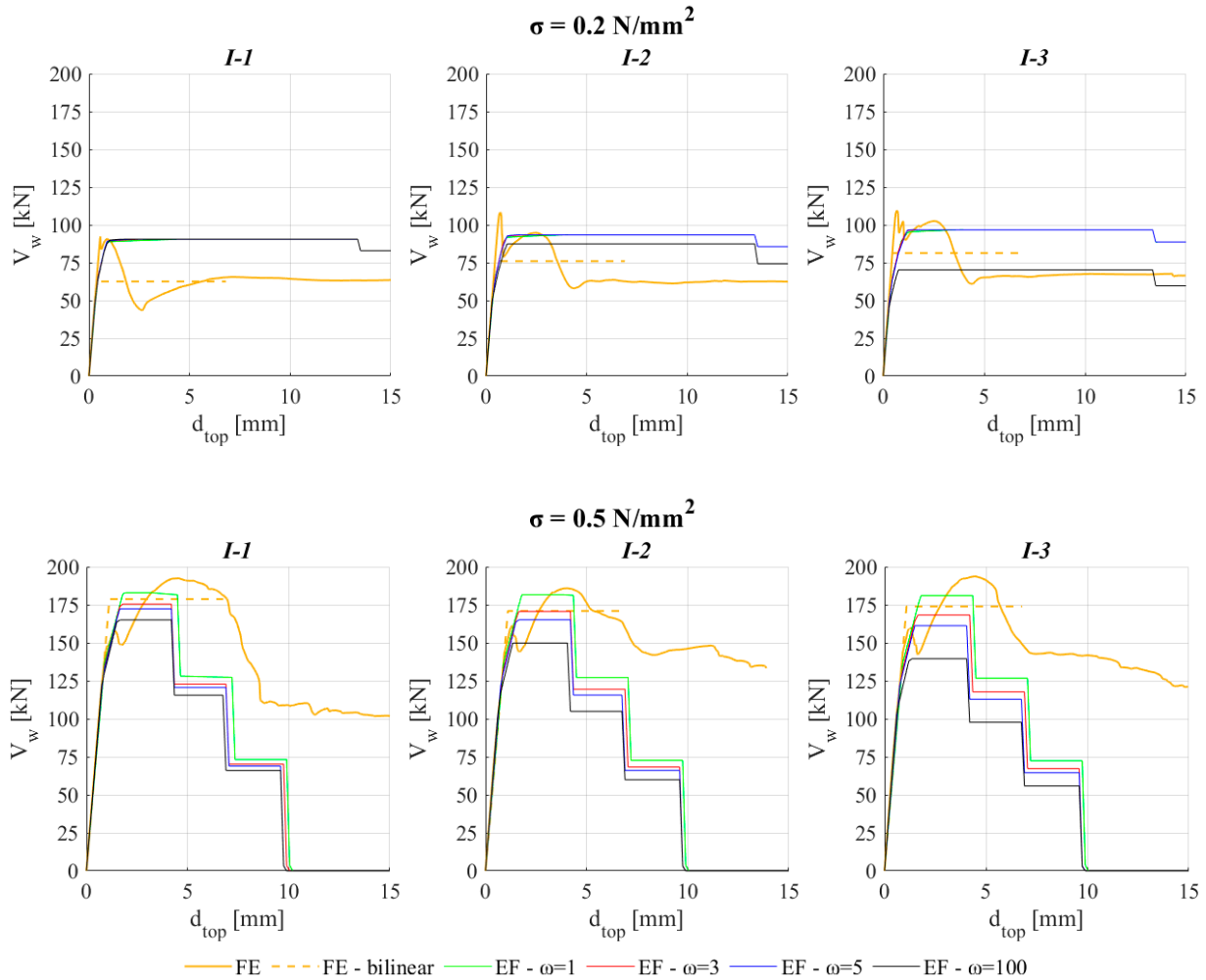


Figure 15. Comparison in terms of web's base shear (V_w) versus horizontal top displacement (d_{top}) curve for some of the examined I-shaped 3D assemblies.

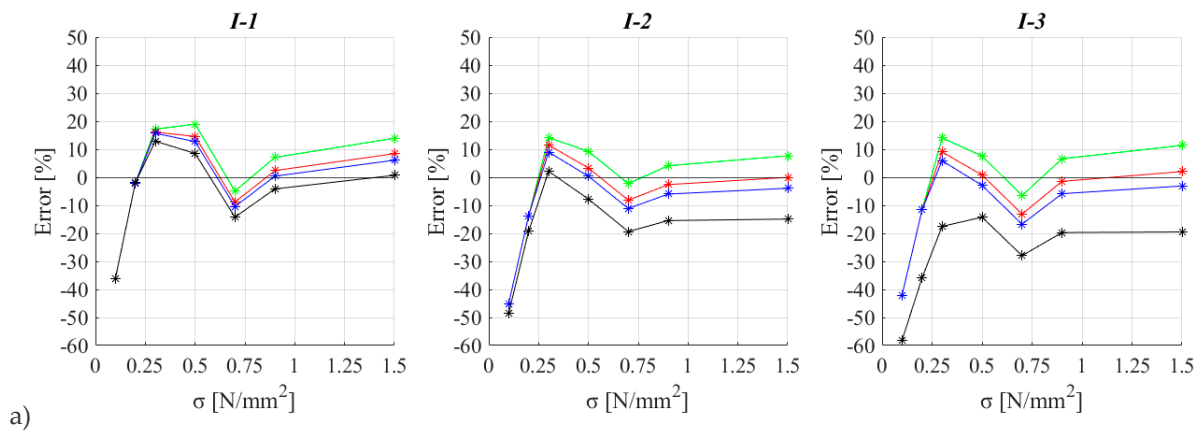


Figure 16. Cont.

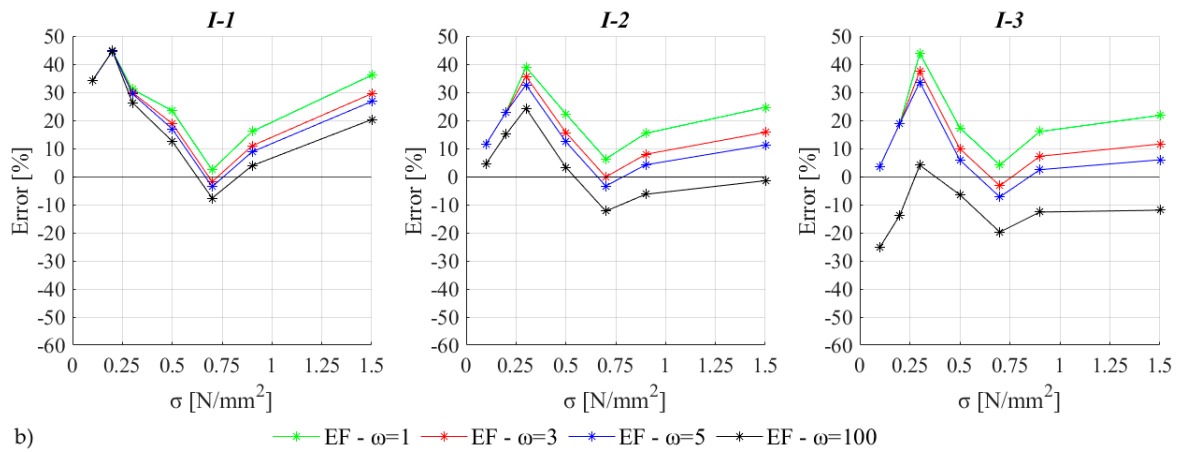


Figure 16. Percentage error of the estimate of the base shear provided by the EF model computed with respect the maximum base shear (a) or the equivalent yield base shear (b) of the FE model.

Finally, Figures 17 and 18 illustrate some results for the case of the T-shaped 3D assemblies. The format adopted is analogous to Figures 12 and 13. The results substantially confirm what was already discussed in the case of the I-shaped system, although for the T-shaped one the influence on the ω choice appears relevant only on the initial axial force estimate. Moreover, in this case, the reference value, which allows for the reproduction of the redistribution of the FE model, is between 3 and 5.

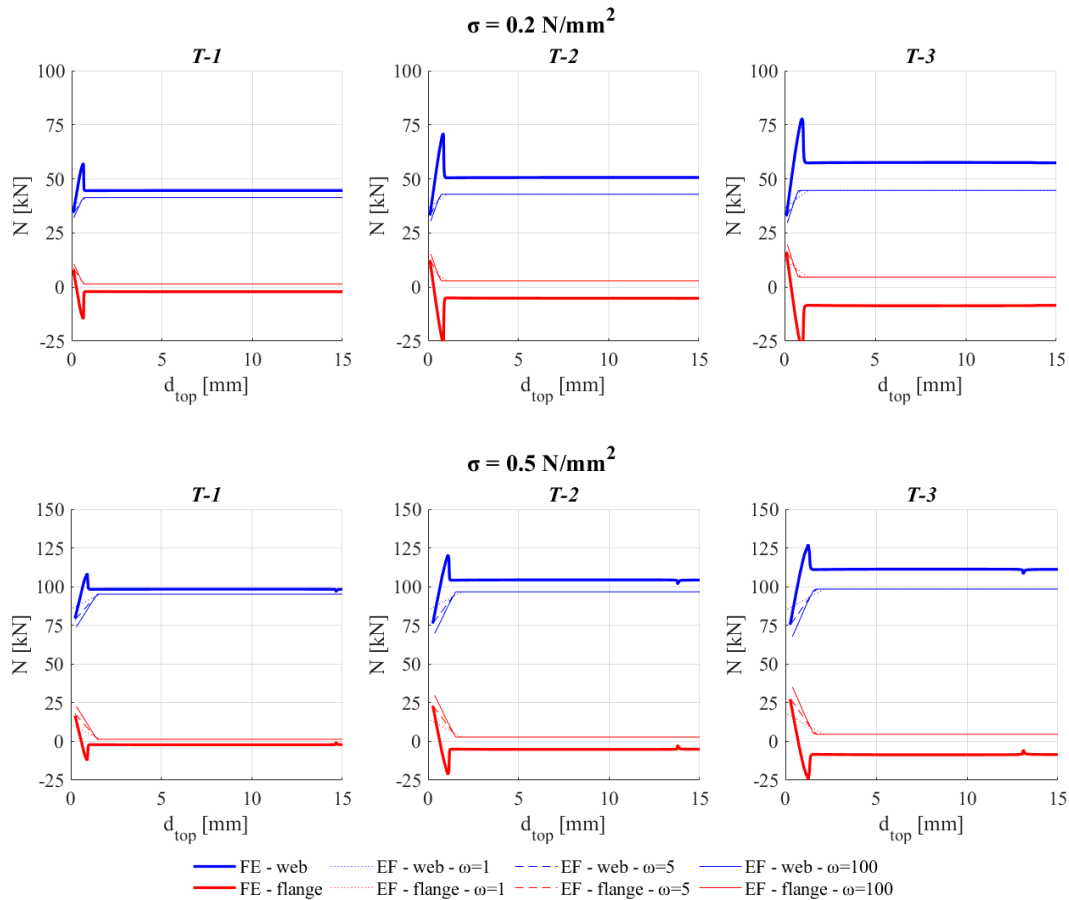


Figure 17. Comparison between FE and EF models in terms of variation of the axial loads on the three components of T-shaped 3D assemblies.

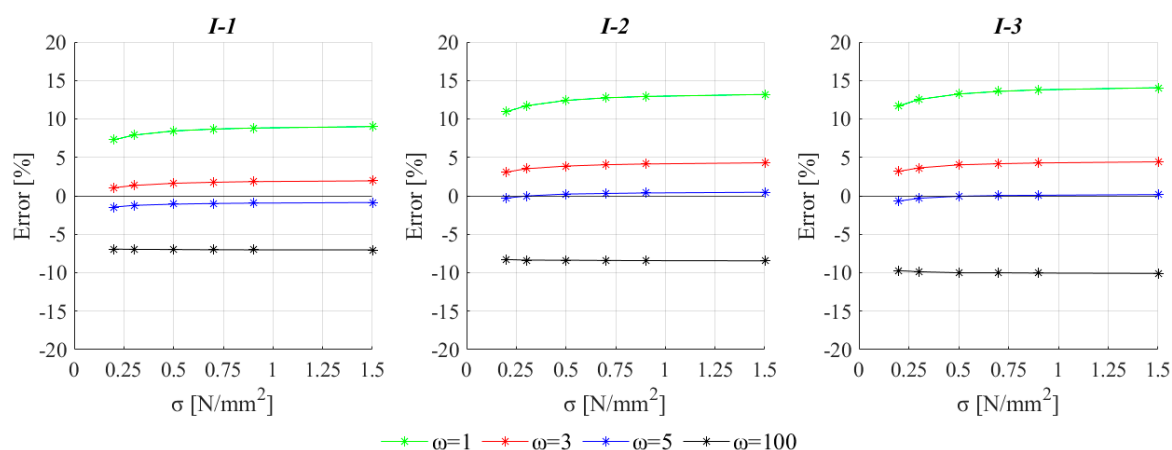


Figure 18. Percentage error on the estimate of the axial load after the application of vertical loads ($d_{top} = 0$) for the examined T-shaped 3D assemblies.

6. Application of the Formulation to Complex Systems

The strategy outlined in the previous sections has been implemented for the pushover analysis of two complex buildings with the aim of exemplifying how the proposed value of the parameter ω is appropriate for the calibration of the flange effect in EF numerical models aimed to the seismic assessment of existing URM buildings. The case studies, namely the Pizzoli's town hall and the former courthouse of Fabriano (Figure 19), consist of two structures instrumented by a permanent accelerometric monitoring system [52,53], which were hit by the Central Italy 2016/17 earthquake. Very accurate data on the structural details and the actual seismic response were available for both buildings, which are dominated by a box-type behavior and characterized by a good wall-to-wall connection. The two-story Pizzoli's town hall is made by cut stone with running bands in solid bricks and floors made by steel beams and hollow flat blocks with r.c. infill; moreover, r.c. ring beams are present at both levels. The four-story former courthouse of Fabriano presents an irregular plan; the walls are made of regular masonry of three different typologies (stone masonry, solid-brick masonry, and stone masonry with an external brick face, named as M1/M2/M3 in Figure 19), while the horizontal diaphragms are of four typologies, which mostly combine H steel beams with various types of hollow brick elements and RC slabs. For both buildings, EF numerical models were available, previously developed by the authors through the Tremuri software [34].

Figure 20 illustrates the equivalent frame idealization of some walls of both numerical models, where the equivalent beams connecting the piers with the flanges are also visible. The masonry panels where the nonlinear behavior is concentrated are the elements in orange (the piers, vertical elements) and green (the spandrels, horizontal masonry coupling beams), while the cyan portions correspond to rigid nodes. Further information is available in [39,54,55] for the Pizzoli's town hall and in [38], for the former courthouse of Fabriano. In particular, an in-depth investigation of the various aleatory and epistemic uncertainties, which intrinsically may affect the numerical modeling and the validation of models against the available experimental data (i.e., ambient vibration measurements and recordings of real seismic events), has been carried out. Starting from these models, in this paper, the shear connections between intersecting piers are estimated by adopting the analytical approach presented in Section 3 and by verifying the sensitivity of achievable results to different values of the parameter ω . Of course, once the proper modeling of the flange effect is obtained, on the basis of the geometric and structural details of the 3D assemblies, a further refinement of the model calibration would be necessary to improve the structural dynamic identification, but this is out of the scopes of the paper.

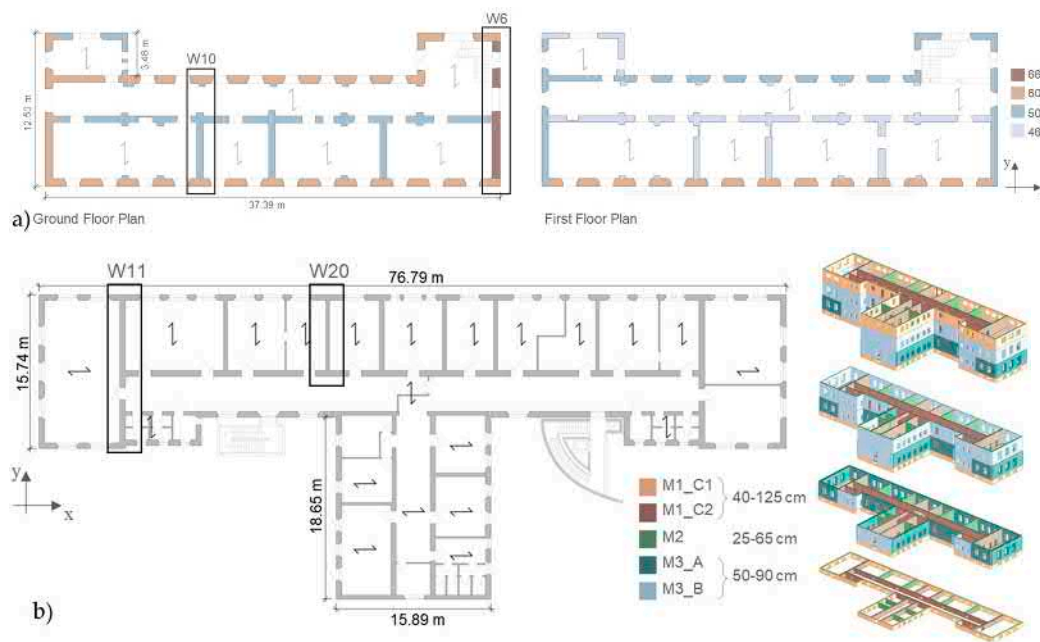


Figure 19. In-plan view of the Pizzoli’s town hall (a) and the former courthouse of Fabriano (b) with the indication of wall’s thickness and location of various masonry types.

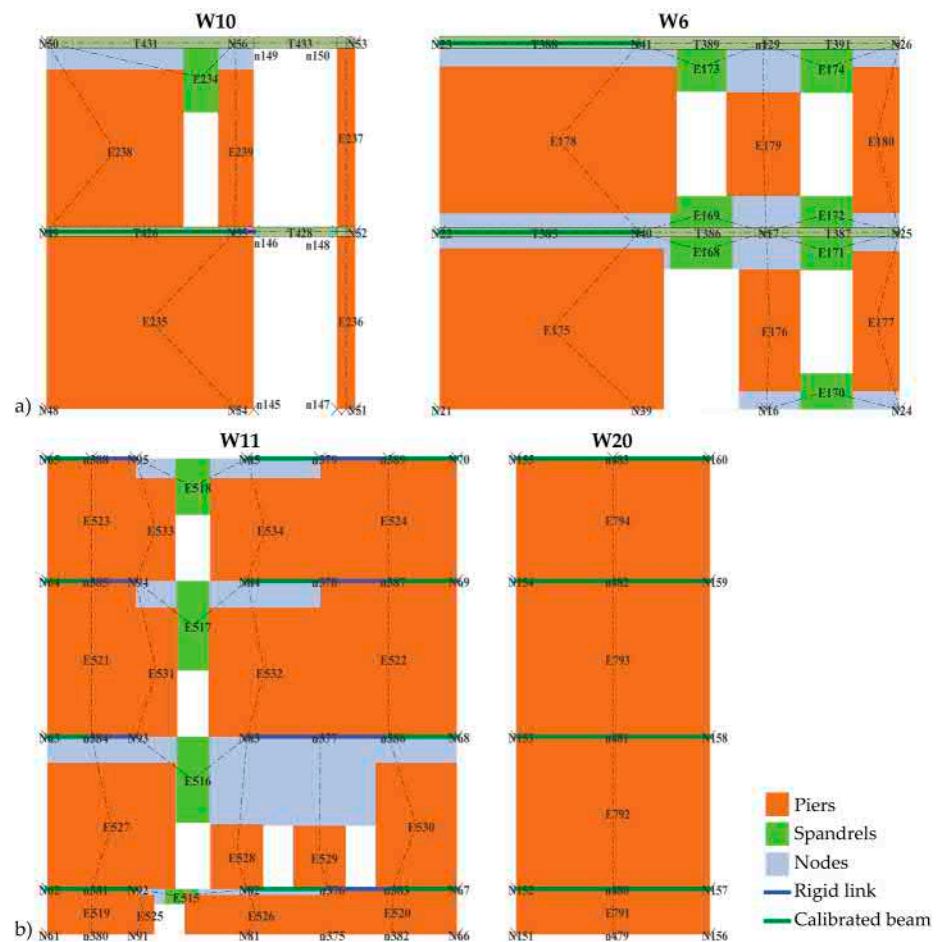


Figure 20. Examples of equivalent frame idealization for some walls of numerical models of Pizzoli town hall (a) and the former courthouse of Fabriano (b) (the walls are those marked in Figure 19).

Figures 21 and 22 illustrate the sensitivity of the dynamic properties of numerical models in terms of either error on the natural frequency estimate and Modal Assurance Criterion (MAC, [56]), for the first five modes; for both comparisons, the target reference consists of the data available from the ambient vibration measurements carried out by the Department of Civil Protection once the monitoring system was installed and made available in previous research [53]. It is worth recalling that values of MAC as close as possible to 1 indicate a good match between experimental and numerical data. In particular, the following values of ω have been investigated:

- The value 100, which has proven equivalent to the limit case of rigid link coupling elements or full vertical coupling (in fact, it has been verified that achieved results are analogous to this modeling option). This value may potentially be responsible for overestimating the flange effect;
- The value of 5, which is the reference value proposed to be representative of a good wall-to-wall connection, on the basis of the results discussed at Section 4;
- The value of 1, which is assumed as the first tentative value for the case of a poor wall-to-wall connection;
- The value of 0.1, which has been proven equivalent to the limit case of the full decoupling of intersecting elements (in fact it has been verified that a further decrease does not affect the results more).

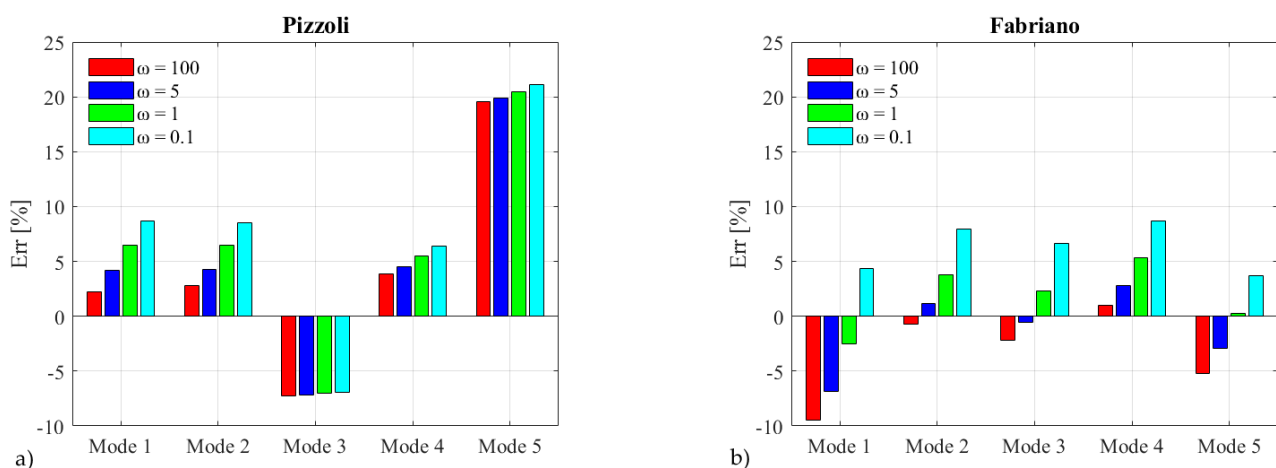


Figure 21. Errors on the estimate of natural frequencies of first five modes varying the ω value from 100 to 0.1: (a) Pizzoli's town hall; (b) former Fabriano courthouse.

As already mentioned, the actual structural details of the two buildings justify the adoption of a good wall-to-wall connection; thus, it is expected that the assumption of ω equal to 5 is the more reliable for these case studies. As a confirmation of that, this value is the one that minimizes the error and maximizes the MAC values. This is particularly evident for the former courthouse of Fabriano, for which moving away from 5 makes the results worsen significantly, both in terms not only of frequency errors but also of modal shapes. The Pizzoli's case study appears less sensitive to ω at least in the elastic range; that emerges particularly from the check on modal shapes, which are almost insensitive to ω .

Figures 23 and 24 instead show the sensitivity to ω in the case of nonlinear static analyses (pushover curves) carried out in X and Y directions, respectively, and by assuming a horizontal load pattern proportional to masses. It may be observed how the base shear strength capacity of Pizzoli's case study is significantly affected by the degree of flange connection. The amount of variation in the results depends also on the specific architectural configuration of the buildings and on the role of piers mostly affected by the flange effect in equilibrating the external forces. To better investigate this issue and by referring to the Y direction, Figure 25 shows the results of the case studies of Fabriano's (a) and Pizzoli's (b), respectively:

- On the top, the variation on the axial force acting on the piers after the application of vertical loads in the cases in which ω is equal to 100 (in red) or 0.1 (in blue) measured with respect to the case of $\omega = 5$;
- On the bottom, the rate of the horizontal forces equilibrated by each pier (computed in correspondence of the maximum base shear of the pushover curve).

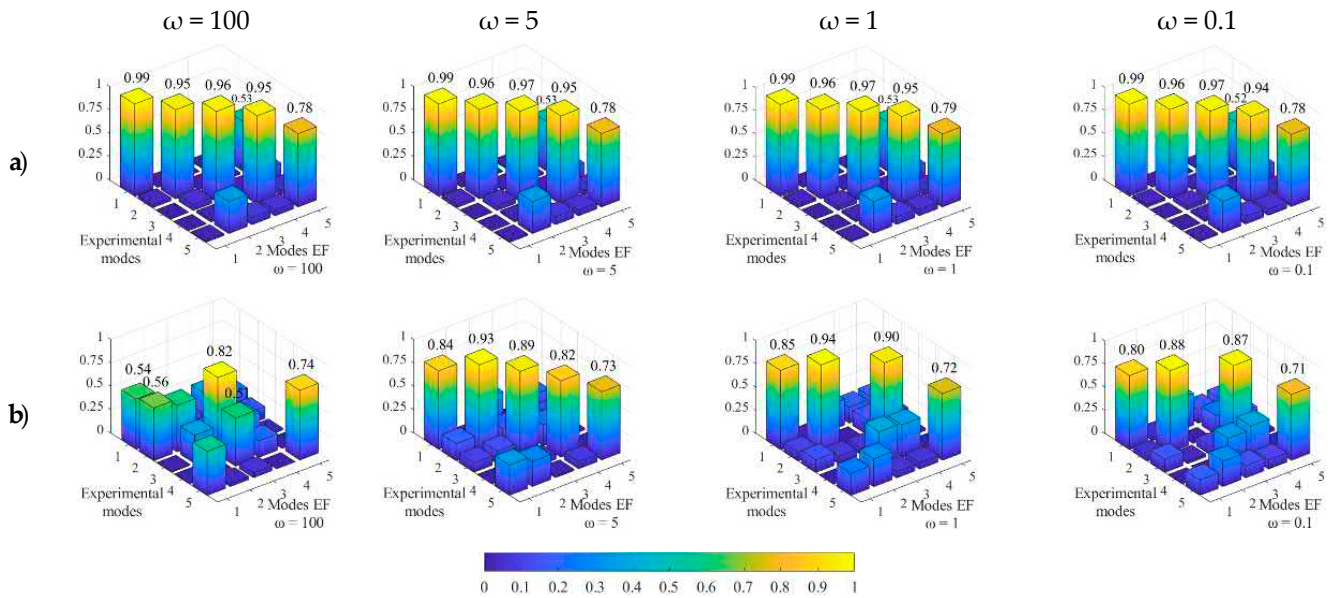


Figure 22. MAC matrixes varying the ω value from 100 to 0.1: (a) Pizzoli's town hall; (b) former Fabriano courthouse.

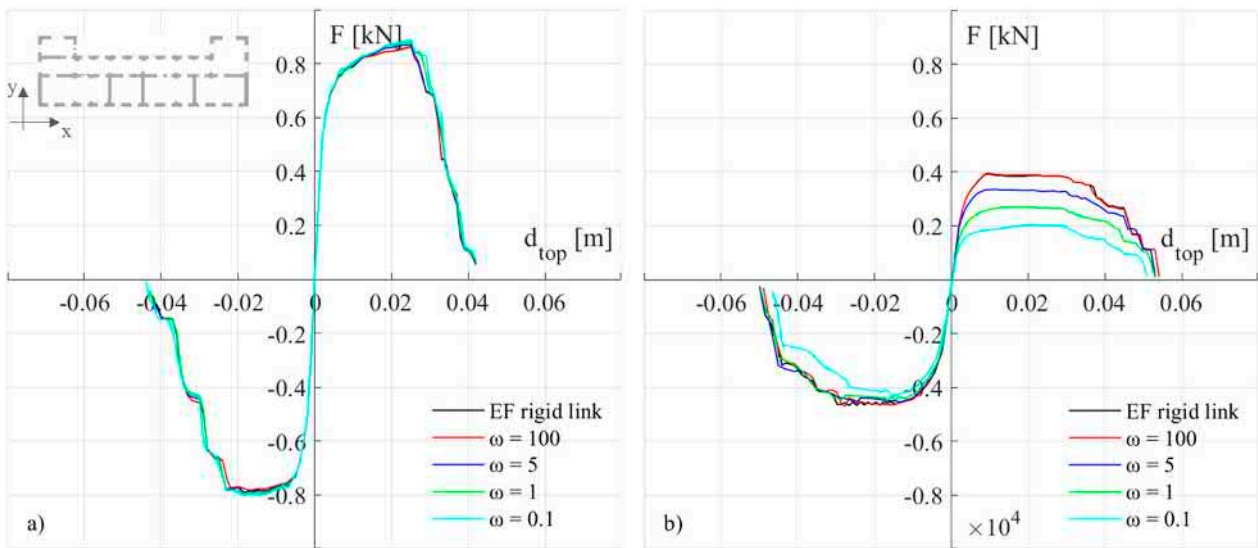


Figure 23. Sensitivity of pushover curves in X (a) and Y (b) directions varying ω values in the case of Pizzoli's town hall.

The results of Figure 25 highlight how in the case of Pizzoli's town hall the piers mostly affected by the axial force redistribution induced by the flange effect are also those carrying most of the shear forces.

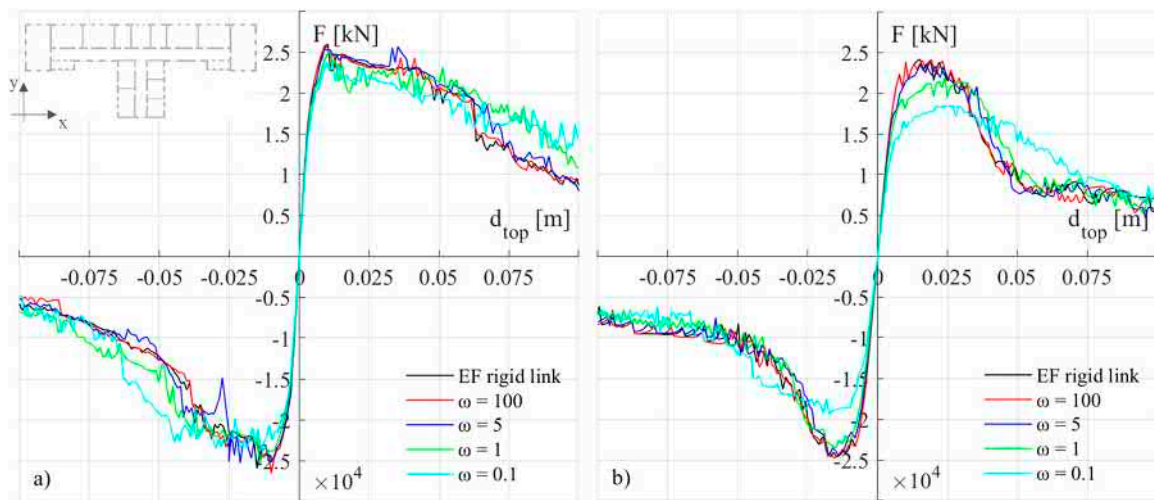


Figure 24. Sensitivity of pushover curves in X (a) and Y (b) directions varying ω values in the case of former courthouse of Fabriano.

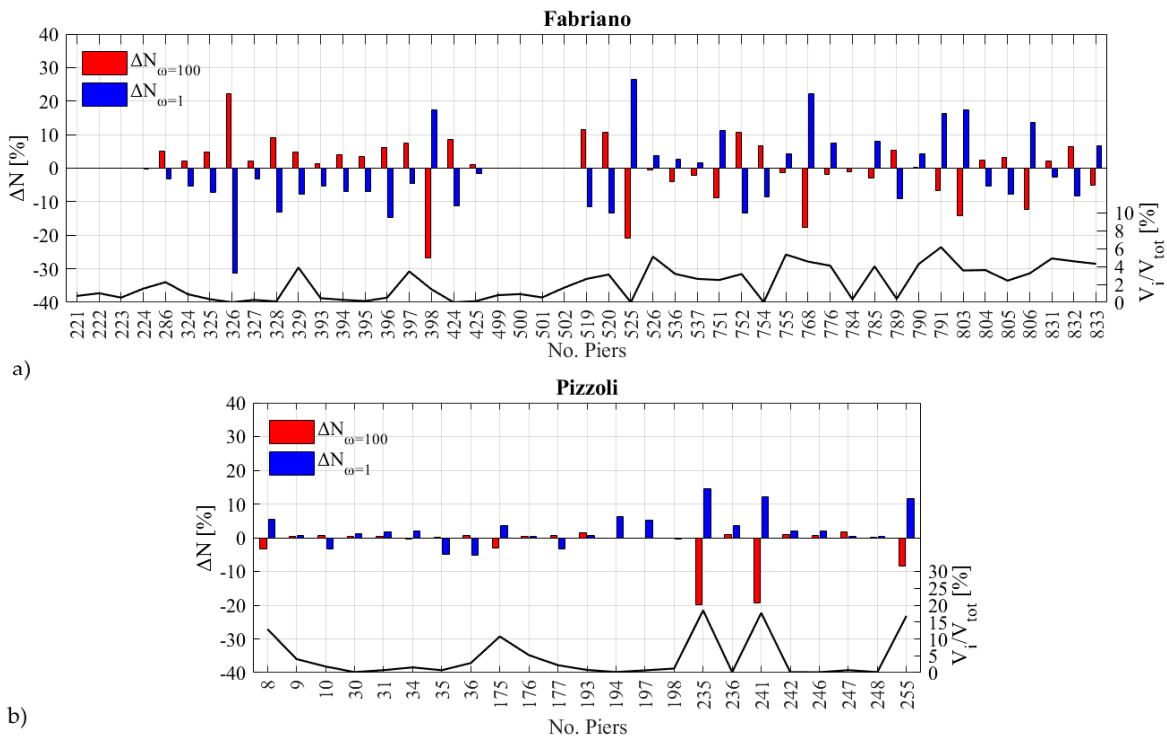


Figure 25. Variation on the axial force acting on piers after the application of vertical loads (on the top, left axis) and rate of horizontal forces equilibrated by each pier respect to the maximum base shear of the overall pushover curve (on the bottom, right axis). Results refer to the former Fabriano courthouse (a) and the Pizzoli’s town hall (b).

7. Conclusions

Firstly, the interpretation of the results obtained on simple flanged systems by the FE approach allowed the demonstration that the failure domains employed for describing the maximum strength of in-plane loaded panels are still effective even if reference is made to the rectangular cross-section of the web. This is valid under the assumption to be able to correctly capture the vertical load redistribution between the web and the flanges and so to correctly estimate the axial load acting on the web panel. The results suggest that further investigations on the reliability of strength domains are only necessary in the

case of low values of axial load and significant dimensions of the flange, since in these situations the rocking phenomenon in the web panel may be altered. In these cases, the maximum strength detected in the web panel does not follow the failure criterion referring to the flexural failure in the associated strength domain but is closer to the shear failure criterion. This suggests that only the criterion for shear failure should be considered if a compressed flange is present. However, this topic should be further investigated before a robust proposal for practice-oriented applications.

The above-mentioned outcomes have suggested the possibility of modeling the flange effect in EF models by connecting intersecting piers by an equivalent beam with a properly calibrated shear stiffness, to reproduce the correct vertical load redistribution and, consequently, the shear strength.

A practice-oriented analytical formulation has been proposed to evaluate the stiffness of the equivalent connecting beam, as a function of the geometric features of the web and the flanges of the 3D assembly of masonry piers. An extended parametric analysis has been performed to validate the effectiveness of the proposed formulation, through a comparison with accurate nonlinear FE analyses of different 3D assemblies. The dimensionless ω parameter is the key factor to correctly redistribute the vertical load, and the reference value equal to 5 may be used in all cases.

It is worth noting that the proposed formulation is aimed to calibrate the contribution of flanges connected to masonry panels (piers) that are in-plane loaded, in the case of a good interlocking between the intersecting piers. A rigid connection would overestimate the flange effect (when the flange is very big with respect to the web) while the proposed elastic stiffness of the equivalent beam can account for the contribution provided by the “so-called” effective width of the flange.

The sensitivity of the global response of masonry buildings to the quality of the wall-to-wall connection was also investigated since, in old masonry buildings, a bad or intermediate interlocking between intersecting piers is often present, since masonry walls are often of different types (i) or made at different times (ii) or already cracked (iii). Typical examples of (i) and (ii) consist of perimetral walls made of irregular masonry (e.g., by stone blocks) and internal walls of regular masonry (e.g., made by solid or hollow bricks). Instead, cracks typical of the case (iii) may be the consequence both of foundation settlements or damage induced by seismic events (in some cases also of low–moderate entity). To model this issue, the shear stiffness of the connecting equivalent beam should be reduced with respect to that provided by the proposed formulation. This may be obtained by introducing a second shear stiffness, in series with the one of Equation (3), or by properly reducing the dimensionless parameter ω . The preliminary investigations made in this paper suggest the adoption of a value equal to 1 for the case of intermediate–poor connections and 0.1 for simulating the condition of perfect decoupling.

The results here obtained allow us to provide some useful directions that could be considered in the EF models and towards which the future development of this research will be addressed. Parametric analyses have been performed on piers with symmetrical I-shaped cross-sections, but the piers included in a real masonry building may also have C-, L-, and T-shaped cross-sections; therefore, these situations should also be investigated to further confirm or extend these considerations.

Author Contributions: S.C.: conceptualization, supervision, result interpretation, funding, and writing—original draft preparation; S.A.: modeling and analysis, result post-processing, figure editing, and writing—original draft preparation; S.L.: conceptualization, supervision, software, and writing—review. All authors have read and agreed to the published version of the manuscript.

Funding: Italian Ministry of Education, University and Research (MIUR) within the DETECT-AGING—“Degradation Effects on Structural Safety of Cultural Heritage constructions through simulation and health monitoring” project (Protocol No. 201747Y73L).

Data Availability Statement: Not applicable.

Acknowledgments: This research has been supported by the Italian Ministry of Education, University and Research (MIUR) thanks to the funded project of national interest DETECT-AGING—“Degradation Effects on Structural Safety of Cultural Heritage constructions through simulation and health monitoring” (Protocol No. 201747Y73L). The authors acknowledge Daniela Camilletti for the initial setting of some of the numerical models and preliminary analyses carried out.

Conflicts of Interest: The authors declare no conflict of interest.

References

1. Bracchi, S.; Rota, M.; Magenes, G.; Penna, A. Seismic assessment of masonry buildings accounting for limited knowledge on materials by Bayesian updating. *Bull. Earthq. Eng.* **2016**, *14*, 2273–2297.
2. Bracchi, S.; Rota, M.; Penna, A.; Magenes, G. Consideration of modelling uncertainties in the seismic assessment of masonry buildings by equivalent-frame approach. *Bull. Earthq. Eng.* **2015**, *13*, 3423–3448. [[CrossRef](#)]
3. Cattari, S.; Camilletti, D.; Lagomarsino, S.; Bracchi, S.; Rota, M.; Penna, A. Masonry Italian Code-Conforming Buildings. Part 2: Nonlinear Modelling and Time-History Analysis. *J. Build. Eng.* **2018**, *22*, 2010–2040. [[CrossRef](#)]
4. Tomic, I.; Vanin, F.; Beyer, K. Uncertainties in the seismic assessment of historical masonry buildings. *Appl. Sci.* **2021**, *11*, 2280. [[CrossRef](#)]
5. Ottonelli, D.; Manzini, C.F.; Marano, C.; Cordasco, E.A.; Cattari, S. A comparative study on a complex URM building: Part I—Sensitivity of the seismic response to different modelling options in the equivalent frame models. *Bull. Earthq. Eng.* **2022**, *20*, 2115–2158.
6. Haddad, J.; Cattari, S.; Lagomarsino, S. Use of the model parameter sensitivity analysis for the probabilistic-based seismic assessment of existing buildings. *Bull. Earthq. Eng.* **2019**, *17*, 1983–2009.
7. Martakis, P.; Reuland, Y.; Imesch, M.; Chatzi, E. Reducing uncertainty in seismic assessment of multiple masonry buildings based on monitored demolitions. *Bull. Earthq. Eng.* **2022**, *20*, 4441–4482. [[CrossRef](#)]
8. Cattari, S.; Magenes, G. Benchmarking the software packages to model and assess the seismic response of unreinforced masonry existing buildings through nonlinear static analyses. *Bull. Earthq. Eng.* **2022**, *20*, 1901–1936. [[CrossRef](#)]
9. D’Altri, A.M.; Sarhosis, V.; Milani, G.; Rots, J.; Cattari, S.; Lagomarsino, S.; Sacco, E.; Tralli, A.; Castellazzi, G.; de Miranda, S. Modeling strategies for the computational analysis of unreinforced masonry structures: Review and classification. *Arch. Comput. Methods Eng.* **2020**, *27*, 1153–1185.
10. Russel, A.P.; Ingham, J.M. Flange effects of an unreinforced masonry wall subjected to pseudo-static in-plane seismic forces. In Proceedings of the 14th World Conference on Earthquake Engineering, Beijing, China, 12–17 October 2008.
11. Russel, A.P.; Ingham, J.M. The influence of flanges on the in-plane seismic performance of URM walls in New Zealand buildings. In Proceedings of the New Zealand Society of Earthquake Engineering Conference, Wellington, New Zealand, 26–28 March 2010; p. 38.
12. Russell, A.P.; Elwood, K.J.; Ingham, J.M. Lateral force-displacement response of unreinforced masonry walls with flanges. *J. Struct. Eng.* **2014**, *140*, 04013087.
13. Khanmohammadi, M.; Benham, H.; Marefat, M.S. Seismic behavior prediction of flanged Unreinforced Masonry (FURM) walls. *J. Build. Eng.* **2014**, *18*, 759–784.
14. Sajid, H.U.; Mohammad, A.; Qaisar, A.; Sikandar, H.S. Effects of vertical stresses and flanges on seismic behavior of unreinforced brick masonry. *Eng. Struct.* **2018**, *155*, 394–409. [[CrossRef](#)]
15. Kallioras, S.; Grottoli, L.; Graziotti, F. Quasi-static cyclic tests on U-shaped unreinforced masonry walls made of calcium-silicate bricks and blocks. In *EUCENTRE Research Report EUC092/2020U*; EUCENTRE: Pavia, Italy, 2020.
16. Tomažević, M. The computer program POR. In *Report ZRMK*; Institute for Testing and Research in Materials and Structures: Ljubljana, Slovenia, 1978. (In Slovenian)
17. Costley, A.C.; Abrams, D.P. *Dynamic Response of Unreinforced Masonry Buildings with Flexible Diaphragms*; NCEER-96-0001; University of Buffalo: Buffalo, NY, USA, 1996.
18. Paquette, J.; Bruneau, M. Pseudo-dynamic testing of unreinforced masonry building with flexible diaphragm. *J. Struct. Eng.* **2003**, *129*, 708–716. [[CrossRef](#)]
19. Moon, F.L.; Yi, T.; Leon, R.T.; Kahn, L.F. Recommendations for Seismic Evaluation and Retrofit of Low-Rise URM Structures. *J. Struct. Eng.* **2006**, *132*, 663–672.
20. Bosiljkov, V.; Page, A.W.; Simundic, G.; Zarnic, R. Shear capacity of the flange-web intersections of brick masonry nonrectangular sections. *J. Struct. Eng.* **2010**, *136*, 574–585.
21. Haach, V.G.; Ramalho, M.A.; Corrêa, M.R.S. Parametrical study of unreinforced flanged masonry walls subjected to horizontal loading through numerical modeling. *Eng. Struct.* **2013**, *56*, 207–217.
22. Priestley, M.J.; He, L. Seismic Response of T-Section Masonry Shear Walls. *Mason. Soc. J.* **1995**, *9*, 10–19.
23. Hassan, M.; Ei-Tawil, S. Tension Flange Effective Width in Reinforced Concrete Shear Walls. *ACI Struct. J.* **2003**, *10*, 349–356.
24. Shi, Q.X.; Wang, B. Simplified calculation of effective flange width for shear walls with flange. *Struct. Des. Tall Spec. Build.* **2016**, *25*, 558–577. [[CrossRef](#)]

25. Mordant, C. Unreinforced Clay Masonry Structures: Advanced Characterization of the Seismic Behavior including Acoustic Issues. Ph.D. Thesis, University of Liege, Liège, Belgium, 2016.
26. Yi, T. Experimental Investigation and Numerical Simulation of an Unreinforced Masonry Structure with Flexible Diaphragms. Ph.D. Thesis, Georgia Institute of Technology, Atlanta, GA, USA, 2004.
27. Calderoni, B.; Cordasco, E.A.; Pacella, G.; Sandoli, A.; Musella, C.; Festosi, A. L'influenza del grado di connessione tra le pareti ortogonali sul comportamento sismico degli edifici in muratura. Proceedings of XVIII ANIDIS Conference, Ascoli Piceno, Italy, 15–19 September 2019. (In Italian)
28. EN 1996-1-1, Eurocode 6; Design of Masonry Structures, Part 1: General Rules for Reinforced and Unreinforced Masonry Structures. Comité Européen de Normalisation (CEN): Brussels, Belgium, 2004.
29. MSJC. *Building Code Requirements for Masonry Structures (TMS 402/ACI 530/ASCE 5)*; American Concrete Institute, Structural Engineering Institute, The Masonry Society (Masonry Standard Joint Committee): Boulder, CO, USA, 2008.
30. Milosevic, J.; Cattari, S.; Bento, R. Definition of fragility curves through nonlinear static analyses: Procedure and application to a mixed masonry-RC building stock. *Bull. Earthq. Eng.* **2020**, *18*, 513–545.
31. Vanin, F.; Penna, A.; Beyer, K. Equivalent-Frame Modeling of Two Shaking Table Tests of Masonry Buildings Accounting for Their Out-of-Plane Response. *Front. Built Environ.* **2020**, *6*, 42.
32. Vanin, F.; Penna, A.; Beyer, K. A three-dimensional macroelement for modelling the in-plane and out-of plane response of masonry walls. *Earthq. Eng. Struct. Dyn.* **2020**, *49*, 1365–1387.
33. McKenna, F.; Fenves, G.L.; Scott, M.H. *Open System for Earthquake Engineering Simulation*; University of California: Berkeley, CA, USA, 2000.
34. Lagomarsino, S.; Penna, A.; Galasco, A.; Cattari, S. TREMURI program: An equivalent frame model for the nonlinear seismic analysis of masonry buildings. *Eng. Struct.* **2013**, *56*, 1787–1799.
35. Lubliner, J.; Oliver, J.; Oller, S.; Onate, E. A Plastic-Damage Model for Concrete. *Int. J. Solids Struct.* **1989**, *25*, 299–329. [[CrossRef](#)]
36. Cattari, S.; Lagomarsino, S. Masonry structures. In *Developments in the Field of Displacement based Seismic Assessment*; Sullivan, T., Calvi, G.M., Eds.; IUSS Press: Pavia, Italy, 2013; pp. 151–200.
37. Brunelli, A.; de Silva, F.; Piro, A.; Parisi, F.; Sica, S.; Silvestri, F.; Cattari, S. Numerical simulation of the seismic response and soil-structure interaction for a monitored masonry school building damaged by the 2016 Central Italy earthquake. *Bull. Earthq. Eng.* **2021**, *19*, 1181–1211.
38. Cattari, S.; Degli Abbati, S.; Alfano, S.; Brunelli, A.; Lorenzoni, F.; da Porto, F. Dynamic calibration and seismic validation of numerical models of URM buildings through permanent monitoring data. *Earthq. Eng. Struct. Dyn.* **2021**, *50*, 2690–2711. [[CrossRef](#)]
39. Degli Abbati, S.; Morandi, P.; Cattari, S.; Spacone, E. On the reliability of the equivalent frame models: The case study of the permanently monitored Pizzoli's town hall. *Bull. Earthq. Eng.* **2022**, *20*, 2187–2217.
40. Milani, G.; Valente, M.; Alessandri, C. The narthex of the church of the nativity in bethlehem: A non-linear finite element approach to predict the structural damage. *Comput. Struct.* **2017**, *207*, 3–18.
41. Fortunato, G.; Funari, M.F.; Lonetti, P. Survey and seismic vulnerability assessment of the baptistery of san giovanni in tumba (Italy). *J. Cult. Herit.* **2017**, *26*, 64–78.
42. Castellazzi, G.; D'Altri, A.M.; de Miranda, S.; Chiozzi, A.; Tralli, A. Numerical insights on the seismic behavior of a non-isolated historical masonry tower. *Bull. Earthq. Eng.* **2018**, *16*, 933–961.
43. Casolo, S.; Diana, V.; Uva, G. Influence of soil deformability on the seismic response of a masonry tower. *Bull. Earthq. Eng.* **2017**, *15*, 1991–2014. [[CrossRef](#)]
44. D'Altri, A.M.; Cannizzaro, F.; Petracca, M.; Talledo, D. Nonlinear modelling of the seismic response of masonry structures: Calibration strategies. *Bull. Earthq. Eng.* **2022**, *20*, 1999–2043. [[CrossRef](#)]
45. Cattari, S.; Camilletti, D.; D'Altri, A.M.; Lagomarsino, S. On the use of Continuum Finite Element and Equivalent Frame models for the seismic assessment of masonry walls. *J. Build. Eng.* **2021**, *43*, 102519. [[CrossRef](#)]
46. Calderini, C.; Cattari, S.; Lagomarsino, S. In-plane strength of unreinforced masonry piers. *Earthq. Eng. Struct. Dyn.* **2009**, *38*, 243–267.
47. Magenes, G.; Calvi, G.M. In plane seismic response of brick masonry walls. *Earthq. Eng. Struct. Dyn.* **1997**, *26*, 1091–1112.
48. Turnsek, V.; Sheppard, P. The shear and flexural resistance of masonry walls. In Proceedings of the International Research Conference on Earthquake Engineering, Skopje, Macedonia, 30 June–3 July 1980.
49. NTC18, *Decreto Ministeriale 17/1/2018*; Aggiornamento delle Norme Tecniche per le Costruzioni. Ministry of Infrastructures and Transportation: Rome, Italy, 2018. (In Italian)
50. Camilletti, D. Equivalent Frame Modelling of URM Buildings: Numerical Validation and Rules. Ph.D. Dissertation, University of Genoa, Genoa, Italy, March 2019.
51. Lagomarsino, S.; Morbiducci, R. A new strengthening technique for timber floors: Structural features and technical details. In Proceedings of the 10th National Conference CTE on New Building Technologies for Europe, Milan, Italy, 3–5 November 1994; Volume 1, pp. 275–284. (In Italian)
52. Dolce, M.; Nicoletti, M.; De Sortis, A.; Marchesini, S.; Spina, D.; Talanas, F. Osservatorio sismico delle strutture: The Italian structural seismic monitoring network. *Bull. Earthq. Eng.* **2017**, *15*, 621–641. [[CrossRef](#)]

53. Cattari, S.; Degli Abbati, S.; Ottonelli, D.; Marano, C.; Camata, G.; Spacone, E.; da Porto, F.; Modena, C.; Lorenzoni, F.; Magenes, G.; et al. Discussion on data recorded by the Italian structural seismic monitoring network on three masonry structures hit by the 2016–2017 Central Italy earthquake. *Proc. COMPDYN* **2019**, *1*, 1889–1906.
54. Degli Abbati, S.; Cattari, S.; Lagomarsino, S. Validation of a practice-oriented floor spectra formulation through actual data from the 2016/2017 Central Italy earthquake. *Bull. Earthq. Eng.* **2022**, *20*, 7477–7511. [[CrossRef](#)]
55. Cattari, S.; Angiolilli, M. Multiscale procedure to assign structural damage levels in masonry buildings from observed or numerically simulated seismic performance. *Bull. Earthq. Eng.* **2022**, *20*, 7561–7607.
56. Allemange, R.J.; Brown, D.L. A correlation coefficient for modal vector analysis. In Proceedings of the 1st International Modal Analysis Conference, Orlando, FL, USA, 8–10 November 1982; pp. 110–116.

Disclaimer/Publisher’s Note: The statements, opinions and data contained in all publications are solely those of the individual author(s) and contributor(s) and not of MDPI and/or the editor(s). MDPI and/or the editor(s) disclaim responsibility for any injury to people or property resulting from any ideas, methods, instructions or products referred to in the content.